NTNU

Norwegian University of
Science and Technology

Heat Exchange in a Fluidized Bed Calcination Reactor

Bjørn Simonsen

Master of Science in Energy and Environment
Submission date: July 2008
Supervisor: Per Finden, ELKRAFT

Norwegian University of Science and Technology
Department of Electrical Power Engineering

Problem Description

At the planned HyNor node at Romerike, hydrogen gas is to be produced from solar energy and bio energy. The bio energy which will be used will most likely be land fill gas from the land fill at Bøler in Skedsmo municipality. The hydrogen production unit is planned to be located at the site of Akershus Fjernvarme AS's new central heating plant in Lillestrøm. The hydrogen production from the land fill gas will be carried out via SE-SMR(Sorption Enhanced Steam Methane Reforming).

The main focus of the thesis will be on the SE-SMR reactor. The physical and thermochemical processes are studied closer, with a special emphasis on the regeneration/calcination of the CO2 sorbent which is a central part of SE-SMR, and different ways of providing the necessary heat for the calcination.

In using an appropriate modelling program, the necessary heat exchange in the calcination reactor will be modelled. The model will be based upon parameters from the planned hydrogen production at HyNor Romerike.

Assignment given: 28. January 2008
Supervisor: Per Finden, ELKRAFT

Preface and Acknowledgement

This work was carried out at Institute for Energy Technology (IFE) at Kjeller, in the period of February to July 2008. I would like to thank the following for their help: Per Finden and Øystein Ulleberg for constructive meetings in the process of defining the work and for revisions along the way, Julien Meyer and Kim Johnsen for valuable answers to pressing questions about the details of Sorption Enhanced Steam Methane Reforming. And finally I would like to thank Thomas Førde for help on setting up the problem in COMSOL Multiphysics and for being helpful with commenting on my work.

Kjeller July, 2008

Bjørn Simonsen

Abstract

Sorption Enhanced Steam Methane Reforming (SE-SMR) is a novel way of reforming natural gas to high purity hydrogen gas with in-situ CO_2 capture by the introduction of a CO_2 sorbent. The process is carried out in two steps. In the first step, hydrogen is produced and CO_2 is absorbed by the sorbent. In the second step, the sorbent is exposed to high temperature heat and the CO_2 is released. For the reforming to run continuously, two bubbling fluidized beds (BFB) can be coupled, one working as a reformer and the other one as a regenerator of the CO_2 sorbent. The reformer works at a temperature around 500˚C and the regenerator at around 900˚C. Once the reactions in the reformer are being carried out the reformer works at a near autothermal state due to the exothermic reaction between CO_2 and the sorbent. The regenerator however needs to be continuously supplied with heat to maintain at least 900˚C and for the endothermic calcination reaction of the sorbent to be carried out.

One of the ways of providing heat to the process is by internal heat exchanger tubes. The advantage of using heat exchanger tubes is that no extra gas is added to the gas already in the bed (used interchangeably with reactor), thus not disturbing the volumetric flow and gas composition of the bed. For sequestration purposes, if the gases within the bed are not disturbed by for example nitrogen, N_2, they will be easier to separate and sequester. An analytical calculation of the energy balance of a calcination reactor with horizontal heat transfer tubes was carried out, and the necessary effect was found to be 14.02kW, which equates to a heat exchanger with 96 tubes in 8 rows, taking up 26cm height in the reactor. Transferring heat via exhaust gas through metal tubes does however not yield a high thermal efficiency.

One way of improving the efficiency of the calcinator is burning fuel gas directly in the reactor. This will lead to a direct heat exchange between the exhaust gas and the sorbent. On the other hand will the direct burning with air as an oxidizer lead to high fractions of N_2 in the reactor. Considering that the gas in question in this work is biogas, the release of CO_2 from the combustion is technically carbon neutral. Calculations for the necessary heat exchanger surface area and combustion rate of

methane for the in-reactor combustion alternative have been carried out analytically, and a model of the in-reactor combustion has been established.

At first, a fully fluidized bed model with integrated methane combustion was planned. Due to limitations of the modeling program and conversations with experts on the scope of the work in relation to the time-frame of the thesis, which is more closely discussed in *Appendix H*, the problem was reduced to a fixed bed approximation with "black box" combustion of methane outside the reactor. A heat balance, dependent on the rate of calcination was applied in the finite element modeling program COMSOL Multiphysics, and the resulting temperatures in the reactor were examined on the basis of what kind of fuel gas was used. In the first case, upgraded biogas, or SNG(Sustainable Natural Gas) was used as fuel gas. SNG is ~100% CH_4, and the biogas has a CH_4 content of ~48%. From the model it was seen that the mean temperature of the bed with SNG was 1218K, or 945˚C, and with the biogas the temperature of the bed was 1248K, or 975˚C. The calcination rate was found to be from 72.5 to 86.3% of the optimum. The lower results might be due to the adiabatic flame temperature of the gas and/or the relatively low heat capacity of the gas.

Sammendrag

Absorpsjonsforbedret damp reformering, eller Sorption Enhanced Steam Methane Reforming (SE-SMR), er en ny teknologi for å reformere naturgass til hydrogen med CO_2 fangst integrert i prosessen gjennom innføring av en CO_2 absorbent, i dette tilfellet kalsitt, $CaCO_3$. Prosessen foregår i to trinn; i det første trinnet produseres hydrogen og absorbenten blir mettet med CO_2. I det andre trinnet blir absorbenten eksponert for høytemperatur varme, og CO_2 gassen blir frigjort. For at reformeringsprosessen skal fungere kontinuerlig kan to boblende fluidisert seng reaktorer bli koblet sammen; en fungerende som reformer og den andre som regenerator av absorbenten. Reformeren har en arbeidstemperatur på rundt 500˚C og regeneratoren på rundt 900˚C. Når de termokjemiske reaksjonene i reformeren har blitt satt i gang, arbeider reformeren tilnærmet autotermisk, eller selvforsynt med varme. Regeneratoren må kontinuerlig tilføyes varme for å opprettholde minimum 900˚C for at den endotermiske kalsineringsreaksjonen av absorbenten skal opprettholdes. Regeneratoren kalles også for kalsinator i forbindelse med SE-SMR da regenereringen av absorbenten i utgangspunktet er en vanlig kalsineringsprosess.

En måte å tilføre varme til prosessen på er via interne varmevekslerrør. Fordelen med å bruke rør er at det da ikke tilføres ekstra gass i reaktoren. Med tanke på CO_2 fangst og deponering er dette spesielt viktig, da gasser som nitrogen(N_2) vil kreve ekstra gass-separasjon før eventuell deponering av CO_2. I oppgaven har varmebehovet for å opprettholde en kalsineringsrate tilsvarende en hydrogenproduksjon på 10 Nm^3 i timen blitt regnet ut analytisk, og viste seg å være 14.02kW. Dette tilsvarer en varmeveksler med 96 rør i rader med 8 rør, som vil ta opp 26cm høyde i reaktoren. Å transportere varme gjennom varmevekslerrør gir likevel ikke en optimal termisk effektivitet da bare en liten del av varmen i gassen blir overført til selve reaktoren.

En måte å forbedre den termiske effektiviteten på er åpen forbrenning av en gass i reaktoren. Dette vil føre til direkte varmeoverføring mellom brenselgassen og absorbenten, men vil samtidig føre til høye fraksjoner av N_2 i reaktoren. Med tanke på at brenselgassen i dette tilfellet er biogass, er den i utgangspunktet CO_2 nøytral og kan forsvare direkte forbrenning i reaktor hvis formålet er å maksimere virkningsgraden

til regeneratoren. Kalkulering av nødvendig varmeveksleroverflate og forbrenningsrate av metan for direkte varmeveksling i reaktoren er gjort i oppgava. Det er også utarbeidet en modell for direkte forbrenning i reaktoren.

I utgangspunktet skulle en komplett fluidisert seng modell med integrert forbrenning av metan modelleres. Grunnet begrensninger i modelleringsprogrammet og samtaler med eksperter omkring arbeidets omfang i forhold til tidsrammen til oppgaven, som er nærmere diskutert i *Appendix H*, ble problemet redusert til en fast-seng tilnærming med metanforbrenning utenfor reaktoren. En varmebalanse, avhengig av kalsineringsraten ble implementert i et finite-element modellerings program, COMSOL Multiphysics, og de resulterende temperaturprofilene ble undersøkt på basis av hvilken type gass som ble brukt. I tilfelle I ble oppgradert biogass, også kalt SNG(Sustainable Natural Gas) brukt. SNG er tilnærmet 100% metan. I tilfelle II ble biogass med metaninnhold på 48% brukt. Med den forskjellige brennverdien for disse gassene oppnåes forskjellige resultater, og gjennomsnittstemperaturen ut av reaktorkonfigurasjonene lå på henholdsvis 1218 og 1248 kelvin for biogass og SNG som brensel. Med biogass som brensel yter reaktoren gjennomsnittlig 12% lavere enn med SNG. Kalsineringsraten lå på mellom 72.5% til 86.3% av den optimale raten. Grunner til lavere enn optimal ytelse kan være lav flammetemperatur eller lav varmekapasitet på gassen.

Contents

List of tables:

List of figures:

List of symbols and abbreviations

Latin Symbols:

Symbol	Description	Unit
a_w	Area of heat exchanger surface	m^2
C_i	Molar concentration of species i	mol/m^3
Cp_i	Heat capacity of species i	J/mol·K
D_{AB}	Binary diffusion coefficient between species A and B	m^2/s
D_t	Outer diameter for heating tube	m
H	Enthalpy	J/mole
k	Thermal conductivity	W/m·K
k_D	Rate constant of calcination	m/s
h	Heat transfer coefficient	$W/m^2·K$
h_w	Bed-surface heat transfer coefficient	$W/m^2·K$
h_r	Radiation heat transfer coefficient	$W/m^2·K$
k_e°	Effective thermal conductivity	W/m·K
k_g	Thermal conductivity of gas	W/m·K
k_s	Thermal conductivity of solid	W/m·K
$\dot{m}$	Mass flux	kg/s
M_i	Molar weight of species i	kg/kmol
p	Pressure	Pa
P_{eq}	Equilibrium pressure of CO_2	Pa
P_i	Partial pressure of CO_2	Pa
Q	Heat transfer rate	W
q_i	Flux	m/s
R_c	Rate of calcination	$mol/m^2·s$
r_p	Radius of particles in bed	m
T	Temperature	K/°C
T_b	Temperature of bed	K
T_w	Temperature of submerged area	K
u_{mf}	Minimum fluidization velocity	m/s
w	Weight of calcined dolomite	kg
X_{CaO}	Conversion of CaO	%
Y_i	Molar fraction of species i	mol/mol

Greek Symbols:

Symbol	Description	Unit
∇	Del operator	-
Δ	Difference	-
ε	Voidage	-
ε_b	Emissivity of bed	-
ε_{mf}	Voidage at minimum fluidization	-
ε_w	Emissivity of wall	-
κ_i	Permeability	m^2
μ_g	Viscosity of gas	Pa·s
ϕ_b	Equivalent thickness of gas film around the contact points between particles	-
ρ_s	Density of solid	kg/m^3
ρ_f	Density of gas/fluid	kg/m^3
τ	Tortuosity factor	kg/m^3

List of abbreviations:

BFB	Bubbling Fluidized Bed
CaO	Calcium Oxide
$CaCO_3$	Calcium Carbonate
CFB	Ciculating Fluidized Bed
CH_4	Methane
CO	Carbon monoxide
CO_2	Carbon dioxide
FC	Fuel Cell
H_2S	Hydrogen Sulfide
H_2	Hydrogen gas
H_2O	Hydrogen Oxide, Water
HyNor	The Hydrogen Highway in Norway
ICE	Internal Combustion Engine
IFE	Institute for Energy Technology
MH-TSC	Metal Hydride Thermal Sorption Compression
N_2	Nitrogen gas
Nm^3	Standard cubic meter
OECD	Organisation for Economic Co-operation and Developnent
PEM	Proton Exchange Membrane
PSA	Pressure Swing Adsorption
PV	Photo Voltaic
SHHP	Scandinavian Hydrogen Highway Partnership
SE-SMR	Sorption Enhanced Steam Methane Reforming
SMR	Steam Methane Reforming
SOFC	Solid Oxide Fuel Cell
S/C	Steam-to-Carbon-ratio
WGS	Water Gas Shift
ZEG	ZeroGen

1 Introduction

1.1 An uncertain energy situation

Fossil fuels are becoming more and more expensive as the demand increases rapidly and the production remains stable. Oil prices are currently at a historical high at $146 per barrel Brent Blend [1]. Estimates of future world energy demands predict a 57% rise, with a 95% rise in non-OECD(Organisation for Economic Co-operation and Developnent) countries, and 24% in OECD countries [2]. The world is consuming fossil fuels in general about a hundred thousand times faster than they are being made[3]. Oil companies have lately, despite violent opposition from environmental organizations, resorted to extracting oil from tar-sands to meet the increasing demands. Biofuels have also gotten a heavy upswing during the last five years, and are looked upon as an environmentally sound alternative to fossil fuels. The biofuels are however neither without controversy: an effect of the development of biofuels which has not been anticipated to a large enough extent is that the production of biofuels leads to increased prices of commodity and basic foods, which some places have increased by more than 50 percent [4]. In addition, severe droughts have hit many of the big grain and rice-producers in the world, making the food reserves even scarcer, and pushing prices even further up. Also, big forested areas have been cut down to meet the increased demand of soybeans and palm oil, which both are easily converted to first generation biofuels. Second generation biofuels based on lignocellulistic material are also being introduced on the market. These do not affect the food resources in the same way as the first generation fuels, but the energy contained in the product fuel is still only about half of the energy input [5]. With high prices, decreasing supply and moral dilemmas for conventional and alternative fuels, there is much interest and research on the alternatives.

1.2 Hydrogen as fuel

One of the alternatives to fossil fuels is a move away from the internal combustion engine (ICE) and a move toward fuel cells (FC), which are more efficient in converting energy, as plotted in Figure 1. For fuel cells, clean hydrogen gas gives the best efficiency and the lowest emissions.

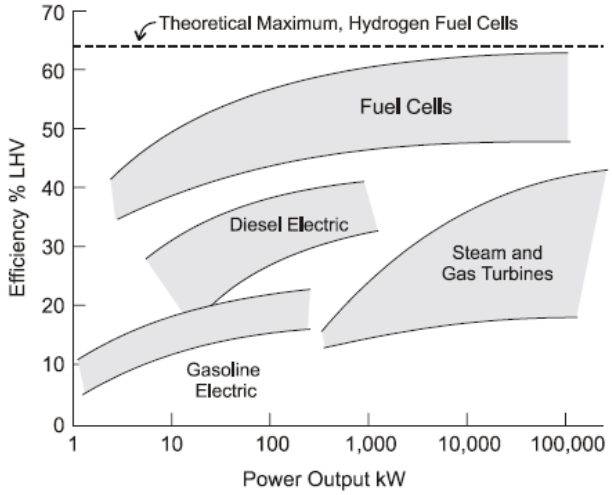

Figure 1: Efficiency vs power output for FC compared to thermodynamic cycles [6]

There have been many issues which in the past favored gasoline as fuel. One among those was the energy storage capacity. With Toyota having successfully tested a car with a 830km range on one filling of high-pressure hydrogen, the storage capacity is no longer a limiting factor [7]. Another factor was the much shorter lifetime of a FC compared to an ICE. That seems to have been solved by 3M, which have a FC membrane that has been running for 7300 hours, or the equivalent of a mileage of 350,000 km [8].

Hydrogen is still an energy carrier, which means energy has to be spent in order to produce it. One of the big advantages with hydrogen as fuel is however that it can be produced from a vast variety of sources. It is found in water, biomass and fossil fuels, and is thus abundant, but bound up in molecules of different characteristics. It is also non-toxic and non-corrosive [9]. With dwindling fossil fuel resources, and an ever smaller amount of countries controlling the petroleum resources, hydrogen can also be considered a “politically neutral” fuel, in the sense that the “oil-countries” do not have an energy monopoly, as the “sources” of hydrogen are more or less equally distributed all over the world in one form or the other.

1.3 HyNor; The Hydrogen Highway in Norway

HyNor is a national project which aims at testing hydrogen as an energy carrier in the transport sector in a market realistic environment. The project was initiated in 2003 and comprises of building a network of hydrogen filling stations with local hydrogen production along the 580km main highway from Stavanger in the southwest of Norway to the Norwegian capital Oslo in the east. As of July 2008, two out of six filling stations are operational; one in Stavanger, and another at Herøya, Grenland. The project goal is to officially open the road in May 2009. Most likely, two additional filling stations will be operational with production facilities by then, and the two last remaining stations will have to get compressed hydrogen transported to them until the local production is up and running. Other Norwegian cities have also expressed interest in joining the network, including Bergen and Trondheim [10]. HyNor is part of the Scandinavian Hydrogen Highway Partnership (SHHP) which will extend the hydrogen highway through Sweden and Denmark to Hamburg, Germany by 2012.

Figure 2: The HyNor project with refueling nodes as planned in 2009[10]

1.3.1 HyNor Romerike

HyNor Romerike can be seen on as an extension of the original HyNor, and will be built in Lillestrøm, a city 20km northeast of Oslo. It is scheduled to be operational within 2010. Lillestrøm is located in Skedsmo municipality, which is part of the

Romerike region. The production facility at HyNor Romerike will incorporate hydrogen production from solar energy and biomass. Photovoltaic (PV) solar panels will produce enough electricity to achieve a hydrogen production of 10 Nm^3 per hour from a high pressure electrolyzer. An additional 10 Nm^3 hydrogen gas per hour will be produced from the reforming of biogas, making the total production capacity 20 Nm^3 H_2 per hour. A metal hydride thermal sorption compressor(MH-TSC) will be used for initial compression of the hydrogen. The reformer will be located on the site of Akershus Fjernvarme AS planned central heating plant in Leiraveien, Skedsmo. The heating plant will use biogas from a local landfill, Bøler Avfallsdeponi, as the base load for the heat production. The SE-SMR will use a branch stream of the land fill gas which will first be desulphurized and upgraded before reforming. At IFE, a SE-SMR reactor has been constructed for research purposes. It is a fluidized bed batch reactor with a maximum production capacity of 10Nm^3/h, and a similar will be constructed for Lindum Ressurs & gjenvinning, who will supply the hydrogen for the HyNor node in Drammen. For more information about the system as a whole and upgrading the biogas, see [11].

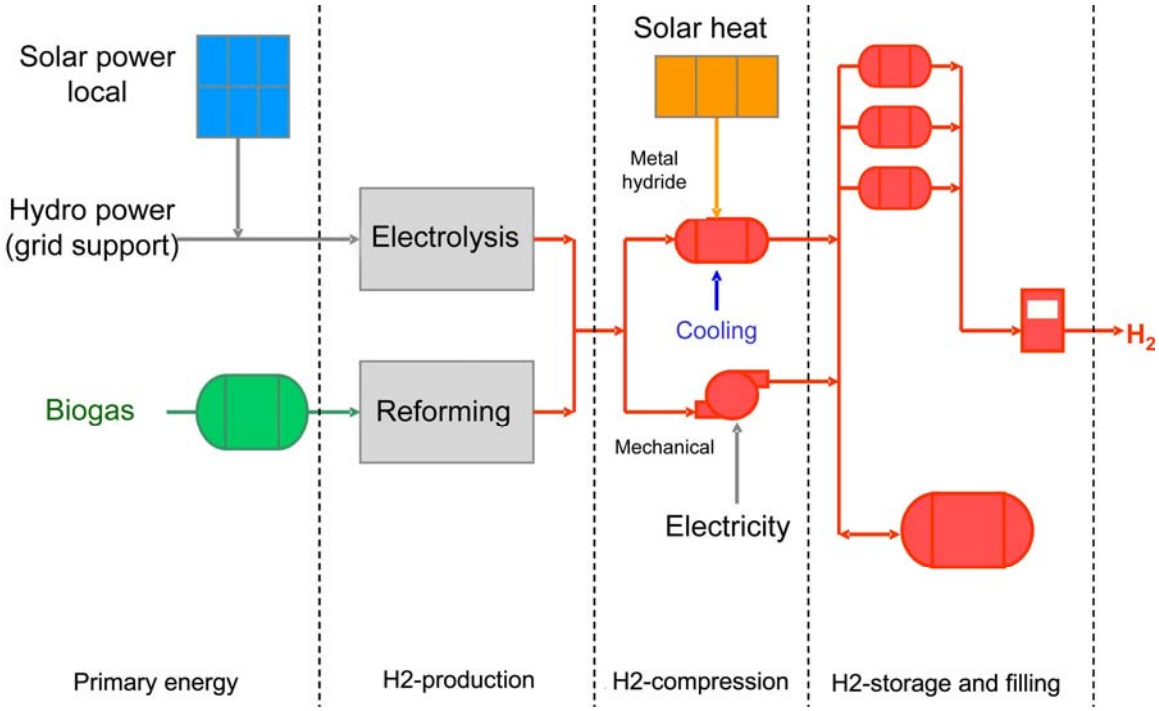

Figure 3: System concept at HyNor Romerike[12]

1.4 Purpose of Work

1.4.1 Thesis Background

Sorption Enhanced Steam Methane Reforming(SE-SMR) is a novel concept of producing hydrogen from natural gas with CO_2 capture included in the process. The CO_2 is captured via absorption on a metal oxide granulate sorbent as the reformation of natural gas is carried out. The sorbent is subsequently exposed to a high-temperature environment where the CO_2 is released as a pure stream, eliminating the necessity of bulky separation equipment downstream. The release reaction of the CO_2, which in practice is a calcination process, is the part of the process which demands the most energy in the form of heat. At IFE (Institute for Energy Technology) there is ongoing research on SE-SMR in a fluidized bed reactor; on different sorbents, catalysts and the operation of the process. In a doctoral thesis on SE-SMR in a fluidized bed, written at IFE by Kim Johnsen [16], he developed a zero-dimensional model of the process, and parts of his work is used as a basis for the development of the two dimensional model presented in this thesis.

1.4.2 Thesis purpose and scope

The aim of this work is looking at different ways of providing the necessary heat for calcination, and establishing a model based on one of the approaches. Two concepts for heat exchange in a fluidized bed are studied in this work. The first concept, a horizontal tube heat exchanger is studied and calculated analytically. The second concept, in-reactor burning of methane or a biogas has been modeled in COMSOL Multiphysics for a fixed- and a semi-fluidized bed. A mathematical model was first established, and then implemented into the modeling program. At HyNor Romerike, either pure or upgraded biogas will be used for hydrogen production, and one of the aims of the modeling is to see whether the burning value of the different biogas compositions is high enough for complete calcination of the sorbent. A work schedule and an evaluation of the schedule are found in *Appendix I*.

1.4.3 Thesis outline

The thesis starts out in *Chapter 1* with brief background information on the HyNor node at Romerike. In *Chapter 2*, the reformation of natural gas is examined. First the standard Steam Methane Reforming (SMR) of natural gas is reviewed. Then the differences and improvements of the SE-SMR process relative to SMR are looked into. *Chapter 3* deals with the calcination/regeneration of the sorbent, and presents the importance of partial pressures and temperatures on the calcination kinetics. In *Chapter 4*, fixed and fluidized beds are presented and compared to eachother, with specific emphasis on the hydrodynamics of the two concepts. The heat exchange in fixed and fluidized beds is examined in *Chapter 5*. In *Chapter 6* a heat balance without considerations of the flow patterns in the calcination process is set up. The mathematical model on which the COMSOL model is based is defined in *Chapter 7*. In *Chapter 8*, a discussion of the dimensioning of the reactor model and the possibilities for integration with parts of the heat plant for mutual heat benefits is looked into. The model description as implemented in COMSOL is presented in *Chapter 9,* while the modeling results are presented and discussed in *Chapter 10*. *Chapter 11* concludes the work and recommendations for further work are briefly presented.

2 Reforming of natural gas

Steam reforming of fossil fuels is currently the least expensive, and thus the most utilized way of producing hydrogen. It accounts for 95% of total production, around half of it from natural gas, and the rest from reforming of oil and coal. At HyNor Romerike, biogas from a local land fill will be utilized. The gas is first cleaned for its sulfurous substances, mainly hydrogen sulfide, H_2S, and is subsequently stripped of its CO_2 and N_2 content. The upgraded product is called "biomethane" or Sustainable Natural Gas (SNG) and is ideally a ~100% pure methane gas. At the local land fill Bøler avfallsdeponi, the biogas has earlier been used for electricity generation, but will now be used as base load for a central heating plant with a branch stream taken out for the reforming to hydrogen.

2.1 Conventional steam methane reforming (SMR)

In conventional SMR, a gas mixture consisting of hydrogen and carbon monoxide is created when steam reacts with methane in the presence of a catalyst at high temperatures (800 – 1000 ˚C) and high pressure (15 – 20 bar). The result is a mixture of hydrogen, and carbon monoxide, carbon dioxide and water; commonly reffered to as *Syngas*. Additional hydrogen is produced in a lower temperature (300 – 400 ˚C) environment by a water gas shift(WGS) reaction with the carbon monoxide. The hydrogen gas is then separated from the CO_2 by pressure swing adsorption (PSA) in several steps until the desired hydrogen purity is achieved [13]. For usage in PEM fuel cells, the CO content should not be higher than ~5ppm [14].

Process steps of conventional SMR:

$$\textit{Reforming: } CH_4(g) + H_2O(g) \leftrightarrow CO(g) + 3H_2(g) \qquad \Delta H = 206\ kJ/mol \qquad (2.1)$$

$$\textit{Shift: } CO(g) + H_2O(g) \leftrightarrow CO_2(g) + H_2(g) \qquad \Delta H = -41\ kJ/mol \qquad (2.2)$$

$$\textit{Overall: } CH_4(g) + 2H_2O(g) \leftrightarrow CO_2(g) + 4H_2(g) \qquad \Delta H = 165\ kJ/mol \qquad (2.3)$$

Despite SMR being widely used for hydrogen production, the process has its disadvantages as listed by Chen et al. [15]:

- Reversibility of reforming reactions and their rapidity constrain hydrogen production to the thermodynamic equilibrium values.
- For minimizing pressure drops, fixed beds must be large, causing the effectiveness of the reforming catalyst to be very low.
- Carbon formation can deactivate the catalyst.
- To maintain high reactor temperatures, heat has to be transferred to and through walls of tubes. (only 50% of the heat of combustion is used directly for the process)
- The process emits NO_x during the burning of fuels in the furnace. CO_2 is also emitted both from furnace and reactor.

2.2 Sorption enhanced SMR (SE-SMR)

The SE-SMR process reduces processing steps by adding a CO_2-sorbent, such as calcium oxide (CaO), which to varying degree is found in calcite and/or dolomite, to the reactor together with the catalyst, absorbing CO_2 as the CO_2 is being produced. This in-situ capture of CO_2 opens for an efficient way of handling the gas for sequestration purposes. When the sorbent, for example calcium oxide, CaO is added to the reactor, the CO_2 is converted to solid carbonate,$CaCO_3$, in an exothermic reaction, resulting in a product gas consisting mainly of H_2 and H_2O, with minor amounts of CO, CO_2 and unconverted CH_4. Adding the sorbent results in other words in a forward shift of reactions (2.1)-(2.3) and thus improves methane conversion and hydrogen yield. The exothermic reaction of carbonation leads to a near autothermal process which operates in temperatures ranging from 550 to 650ºC. In continuous production the carbonated sorbent is subsequently transported to another reactor where it is exposed to high temperature for the endothermic calcination reaction (2.6) to take place. The process steps of a SE-SMR process are identical to the SMR process, but also include the exothermic carbonation equation (2.4):

$$Carbonation:\ CaO(s) + CO_2(g) \leftrightarrow CaCO_3(s) \qquad \Delta H = -178\ kJ/mol \qquad (2.4)$$

Overall: $CH_4(g) + 2H_2O(g) + CaO(s) \leftrightarrow CaCO_3(s) + 4H_2(g)\ \Delta H = -13\ kJ/mol$ (2.5)

Calcination / Regeneration: $CaCO_3(s) \leftrightarrow CaO(s) + CO_2(g)\ \Delta H = 178\ kJ/mol$ (2.6)

In Figure 4 the H_2 concentration is given as a function of temperature. The concentration peaks at 550º C. Sorbent to methane ratio is two, and the steam to carbon(S/C) ratio is 3.

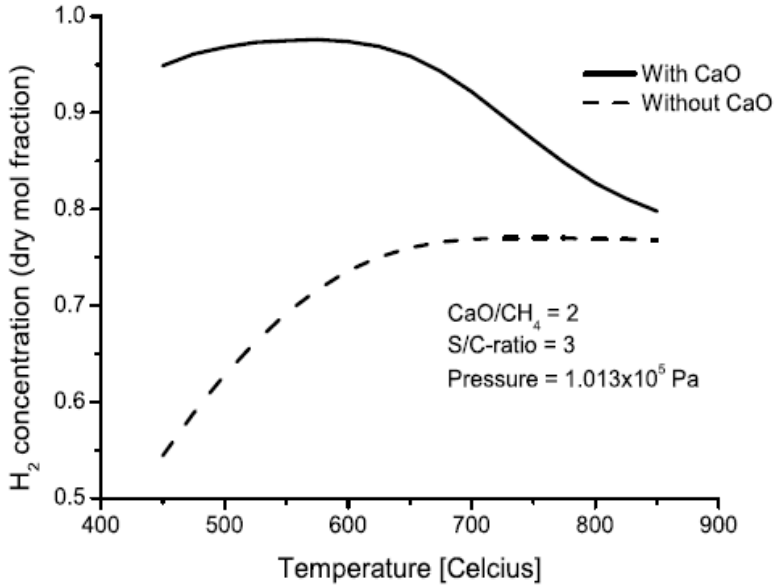

Figure 4: Hydrogen gas fraction as a function of temperature [16]

When most of the available sorbent has been carbonated, H_2 production rate lowers toward standard SMR levels. At a certain point regeneration, or calcination of the sorbent is desired to maintain stable and optimal hydrogen production. Depending on the configuration of the reactor, the sorbent is heated to 900ºC for the endothermic reaction of releasing the CO_2 from the carbonated limestone, $CaCO_3$.

3 Regeneration of the sorbent: calcination

Calcination is a thermal treatment process applied to ores and other solid materials in order to bring about a thermal decomposition, phase transition, or removal of a volatile fraction. The process derives its word from the decomposition of calcium carbonate $CaCO_3$ to calcium oxide or lime, CaO [17]. It is important to understand calcination and its kinetics in order to model it for a SE-SMR process.

3.1 Calcination in a SE-SMR process

For the case of SE-SMR, the sorbent has to continually be regenerated, i.e. the absorbed CO_2 has to be released from the sorbent. This can either be done in the reactor where the reforming is taking place by running the process batch-wise, which has several disadvantages, both operational- and efficiency wise. In a continuous process, two reactors are coupled together and are kept at constant temperatures in order to perform one or the other process of reforming or calcination, with the sorbent circulating between the reactors at a rate proportional with the hydrogen production. The calcination of the sorbent is carried out in a high temperature environment at around 900˚C, which is the decomposition temperature of pure CO_2, given by equation (3.7). Heat delivered to the reactor must both raise the temperature of the carbonated sorbent entering the bed, and provide excess heat sufficient for the calcination reaction to be carried out. At IFE, research in a project called ZeroGen (ZEG) has been carried out. ZEG is briefly explained the coupling of a solid oxide fuel cell (SOFC) with a SE-SMR unit, utilizing the high waste heat from the SOFC to calcinate the sorbent in the SE-SMR process [18]. The equilibrium pressure of CO_2 in the calcinator relates to temperature with the following equation [19]:

$$P_{eq} = 4.137 \cdot 10^7 e^{\frac{-20474}{T}} \tag{3.1}$$

Where the activation energy is 33.4 kJ/mol. When plotted as a function of temperature and pressure, the graph in Figure 5 below is achieved.

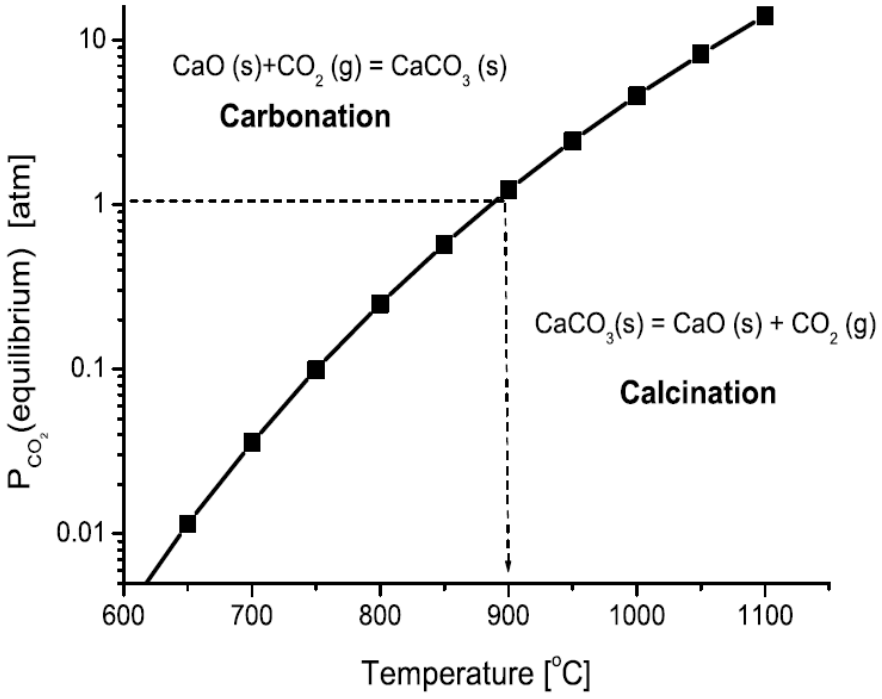

Figure 5: CO_2 equilibrium pressure as a function of temperature [16]

3.2 Calcination kinetics

The rate at which calcination is carried out is vital in order to know what residence time in the calcination reactor is needed. Because of the unique morphology of different sorbents, rate expressions should be calculated for each specific sorbent [16]. Evaluation of calcination kinetics is complicated by CO_2 concentration which is inhibiting the reaction, particle size, which may introduce both thermal and mass transfer limitations, and catalysis or inhibition of impurities. In their review of calcination and carbonation of limestone, Stanmore et.al [19] present the following rate equation for calcination of limestone:

$$R_c = k_D(P_{eq} - P_i)\left[\frac{mol}{m^2 s}\right] \tag{3.2}$$

where P_i is the partial pressure of CO_2 at the reaction surface, P_{eq} is the equilibrium pressure of CO_2 and

$$k_D = 1.22 \exp(-4026/T) \left[\frac{mol}{m^2 s\, atm} \right] \tag{3.3}$$

is the rate constant of calcination.

As can be seen from the calcination reaction (3.2) and (3.3), the calcination rate is dependent on partial pressure of CO_2 in the reactor, and the reactor temperature. One way of increasing the calcination reaction would then be to increase the temperature, which would lead to an increase in the equilibrium pressure. Another way to increase the calcination rate would be to either increase the velocity of the fluidizing gas, which would lead to a lower partial pressure of CO_2 in the reactor, or change the composition of the fluidizing gas.

4 Fixed and fluidized bed reactors

SE-SMR can be carried out in both fixed and fluidized bed reactors. There are many differences between these types of reactors, which will be presented in this chapter. Especially, there will be an emphasis on the hydrodynamics of the different types of reactors due to its importance in heat transfer, which is covered by Chapter 5. At the end of this chapter the importance and implications of the fluidizing medium is examined.

4.1 Fluidized vs Fixed Bed reactors

Fluidized bed reactors, or bubbling fluidized beds have many advantages over the fixed or packed bed, but there are also some disadvantages. The advantages and disadvantages as stated by Kunii & Levenspiel [20] and Chen [21] can be listed as follows:

Advantages of utilizing a fluidized bed:

- The fluidized bed copes much better with highly endothermic or exothermic reactions, whereas in a fixed bed, this can lead to the occurrence of hot- or cold-spots in the reactor.

- Liquid-like behaviour of the particles allows for continuous feeding and withdrawal, and thus continuous operation of the reactor.

- Good mixing which leads to efficient and near isothermal heat distribution.

- Suitable for large scale operations.

- Low pressure drops

- Heat transfer between an immersed body and fluidized bed is big, i.e. heat exchangers within fluidized beds require relatively small area.

The disadvantages of utilizing a fluidized bed:

- Gas by-passing(limited gas-solid contacting)
- Production of solid fines. Mechanical stress on the particles due to the rigorous mixing results in the production of solid fines, which are entrained by the gas, and thus need to be replaced.
- Varying solids residence time distribution due to rapid mixing.
- Erosion on pipes and vessels due to abrasion by particles.
- Higher energy cost due to pumping/pressurizing of fluidizing medium.
- Design and scale-up more complex than with fixed bed.

4.2 Hydrodynamics of fixed bed reactors

In order to characterize the hydrodynamics of a fixed bed, the most important parameters are the voidage and the particle properties. The voidage of the bed is related to the packing arrangement of the bed, which again is directly related to the shape of the particles. The voidage in turn is used together with the fluid velocity to determine pressure drop over the bed, as described by Darcy's Law [22]:

$$q_i = \frac{-\kappa_i}{\mu} \nabla p \tag{4.1}$$

Where q_i is the flux, κ_i is the permeability, μ is the viscosity and ∇p is the pressure gradient. One important factor of Darcy's Law is the permeability. In a fixed bed of particles, the permeability of the bed can be calculated from the Kozeny-Carman equation [21]:

$$\frac{r_p^{\,2}}{\kappa} = \frac{75(1-\varepsilon)}{2\varepsilon^3} \tag{4.2}$$

Where r_p is the radius of the particle, κ is the permeability and ε is the voidage.

4.3 Hydrodynamics of fluidized bed reactors

A fluidized bed reactor is a reactor containing a certain amount of particles, which can be anything from fine powder like flour to bigger ones like coffee beans. The particles are levitated by a stream of gas or fluid entering the bottom of the reactor, passing through a perforated plate or mesh, called the distributor plate before making contact with the particles. Bubbles form above the distributor plate, and coalesce as they move upward to the surface layer of the particles, resembling a boiling liquid. Fluidized beds are utilized for a wide range of appliances. Examples of use are drying food, roasting coffee beans, producing liquid and gaseous fuels etc. The flow rate through the bed is an important parameter, and changes in the volumetric gas flow directly affects the hydrodynamics of the bed [23].

4.3.1 Particle classification

In a reactor containing a certain amount of solid particles, there are many different forms of contacting regimes with a fluid, depending on the fluidization velocity and whether the fluidization agent is gas or liquid. The phases are strongly related to the characteristics of the particles. Geldart(1973) classified particles in relation to their fluidizing properties, and from the Geldart classification, given in *Appendix L*, it is seen that both the catalyst (d_p= 150μm, ρ=2.2 g/cm^3) and the sorbent (d_p= 200μm, ρ=1.6 g/cm^3) are of category B [16], which means they are sand-like and that bubbling in the bed commences at minimum fluidization velocity.

4.3.2 Fluidization phases

Depending on the particles in the fluidized bed and the velocity of the fluidizing gas, distinct fluidizing phases or regimes can be observed. When the fluidizing gas merely percolates through void spaces between stationary particles in a bed, it is said to be *fixed*.

One can look on the physics of the fluidized bed as a two-phase system. At the lower part of the bed, a near uniform mixture of the solids and fluidizing gas is located; also called the *emulsion* or *dense* phase. Excess gas will coalesce into bubbles, henceforth called bubble-phase. Bubbling generally commences at a velocity higher than u_{mf} [24].

4.3.2a Minimum/incipient Fluidization

As the fluidization gas velocity is increasing, the pressure drop also increases, reaches a peak, and then decreases to a stable value as the velocity of the gas keeps increasing. This process is illustrated in *Figure 6*. The point of Δp_b denotes the transition from a fixed to a fluidized bed. The speed at which this transition occurs is called the minimum fluidization velocity, u_{mf}. At this point the frictional force between the particle and fluid counterbalance the weight of the particles, thus suspending them which results in a fluid like behaviour of the particles. From *Figure 6* it can be seen that in the transition from fluidized to fixed bed, the pressure drop follows a different path and does not reach the peak it did in transition from fixed to fluidized bed.

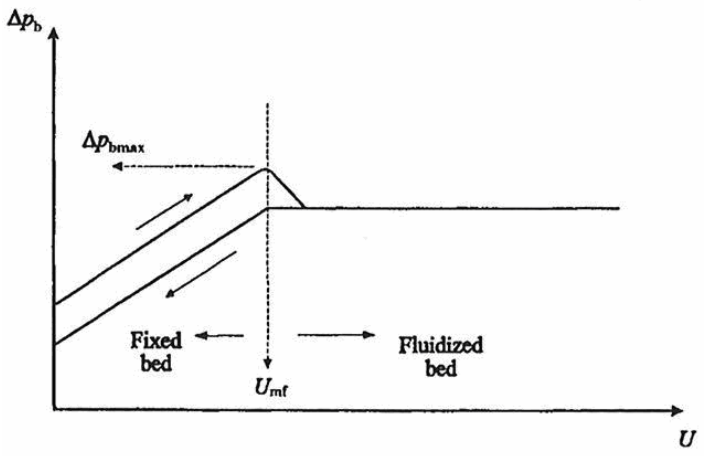

Figure 6: Pressure development as function of gas velocity [25]

4.3.2b Bubbling Fluidization

In a liquid-solid bed, an increase in the velocity above u_{mf} leads to further expansion of the bed and is called *particulate fluidization.* However, in gas-solid systems, large instabilities with bubbling and channelling of gas are observed. The behaviour of bubbles significantly affects the flow or transport phenomena in the bed, including

solids mixing, entrainment, and heat and mass transfer. Bubbles are formed due to the inherent instability of gas-solid systems. Fast local growth in local voidage grows rapidly to a shape resembling a bubble, which can coalesce with other bubbles as it rises to the surface of the bed, bringing along solid fines. The coalescence of bubbles in a gas-solid medium is similar to that of those in a liquid or liquid-solid medium [25]. If the bed is deep and has a small enough diameter, the bubbles may grow large enough to spread across the entire vessel. In the case of fine particles, they flow smoothly down by the wall around the rising void of gas. If the particles are big they are pushed upward as a piston. This is called *slugging*.

4.3.2c Turbulent Fluidization

When the fluidizing velocity exceeds the terminal velocity of the particles, the upper surface of the bed disappears, entrainment becomes appreciable and instead of a dominance of bubble coalescence there is a dominance of bubble break-up and a turbulent motion of solid clusters and voids of gas of various sizes and shapes is observed. A further increase in fluidizing velocity, the solids are carried out of the bed entirely. This phase is called *lean phase fluidization with pneumatic transport of solids*. The fluidizing phases are shown in Figure 7 below.

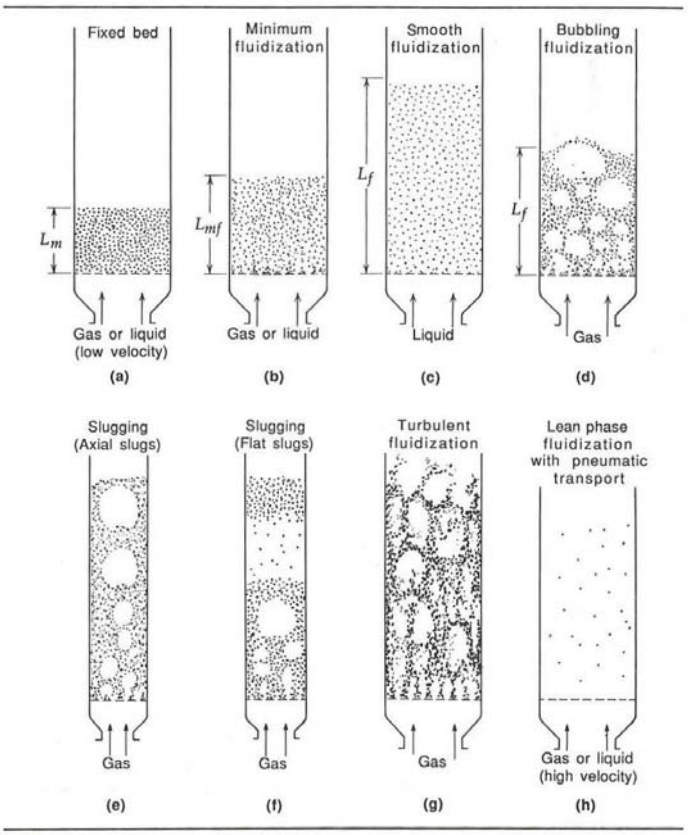

Figure 7: Fluidizing regimes with increasing velocity [20]

4.4 Fluidizing medium

For the process of SE-SMR, there is an emphasis on the ease of extracting the CO_2 from the calcination reactor. In principle CO_2 is the only gaseous product of the calcination reaction. However, the sorbent has to be fluidized by a gas. If this gas is air, CO_2 has to be separated from oxygen and nitrogen downstream. The ideal fluidizing medium for a calciner would thus be steam and/or CO_2 since the steam condenses at a much higher temperature than CO_2 and is thus easily separated from the CO_2. A problem in using CO_2 is that the partial pressure of CO_2 is very high and will make the calcination reaction slower as was discussed in *Chapter 4.2 Calcination Kinetics*. If combustion of methane is carried out in the reactor, extra air is needed and nitrogen will thus be present in the product gas unless it is separated from the oxygen before entering the reactor. The combustion will also lead to an increased amount of CO_2, CO and NO_x, which are all unwanted from an environmental perspective. If pure oxygen used as oxidating agent, another problem arises as the oxygen has an adverse effect on the catalyst.

The ideal fluidizing medium depends mostly on the purpose but also the size of the reactor. If it is a small reactor and the purpose is confirming the feasibility of the SE-SMR process, and regeneration of CO_2, the composition of the medium is not of a big importance. If the purpose however is to demonstrate capture and sequestration of CO_2 in a SE-SMR process, the composition of the fluidizing gas should be optimized for easy downstream separation of CO_2. Also, if the reactor is large, the environmental impact of product gases from both calcination and eventual combustion will have a greater environmental impact and the motivation for sequestering the gases would be larger.

5 Heat exchange in fixed and fluidized beds

Many applications are temperature-dependent, and either needs heating or cooling different from the ambient temperature. The heat transfer characteristics in multiphase systems depend strongly on the hydrodynamics of the systems which, as pointed out in *Chapter 4*, vary significantly with particle properties. The particle size, size distribution and shape affect the particle and fluid flow behavior through particle-fluid and particle-particle interactions. The heat transfer characteristics are strongly influenced by the operating conditions of the fluidized beds. Different operating conditions such as bubbling and spouting yield a varied bed structure and hence varied heat transfer coefficients.

When the bed is in a fixed state, e.g. when the gas velocity is below u_{mf}, the heat transfer coefficient is low. With increasing gas velocity above u_{mf} it increases sharply to a maximum before decreasing slowly [26]. The decrease of h at higher velocities may be attributed to more contact time with bubbles and their low *h* values [20].

5.1 Heat transfer in fixed beds

The principal modes of heat transfer in fixed beds consist of conduction, convection and radiation. The contribution of each of theses modes to the overall heat transfer may not be linearly additive and mutual interaction effects need to be taken into account. In a fixed bed the heat transfer characteristics can be described by the concept of effective thermal conductivity, k_e, which is based on the assumption that on a macroscopic scale the bed can be described by a continuum. It depends on the temperature, the bed material and structure, and is usually determined by evaluating the steady state heat flux between two parallel plates separated by a packed bed. It should be noted that equation (5.1) is derived on the basis that the gas is stagnant:

$$k_e^{\circ} = \varepsilon_{mf} k_g + (1-\varepsilon_{mf}) k_s \tag{5.1}$$

Where ε_{mf} is the voidage, k_g is the thermal conductivity of the gas and k_s is the thermal conductivity of the solid.

To account for actual geometry and the small contact region between adjacent particles, the following modification is added [20]:

$$k_e^{\circ} = \varepsilon_{mf} k_g + (1-\varepsilon_{mf}) k_s \left[\frac{1}{\phi_b (k_s / k_g) + 2/3} \right] \tag{5.2}$$

Where k_e is the effective conductivity, $^{\circ}$ refers to stagnant gas conditions and ϕ_b represents the equivalent thickness of gas film around the contact points between particles, which aids in the transport of heat from particle to particle and is given as a function of k_s/k_g in Figure 8.

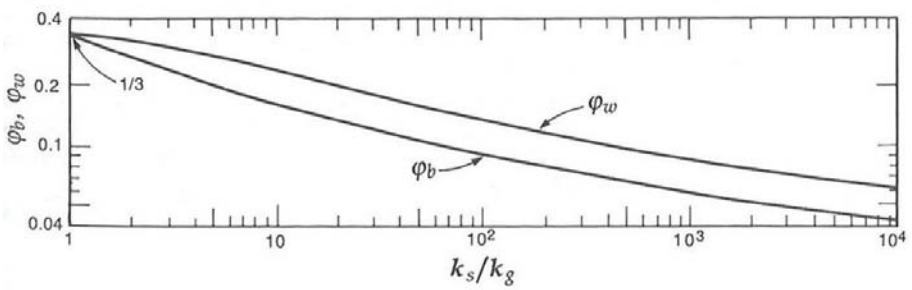

Figure 8: Equivalent thickness of gas film around contact points between particles [20]

5.2 Heat transfer in fluidized beds

One of the big advantages with fluidized beds is its temperature uniformity, both in radial and axial directions. In order to maintain a desired temperature in the bed, a heat exchanger is applied in order to add or remove the appropriate heat [20]. In a fluidized bed there might be heat transfer between gas and particles and/or heat transfer between a static surface and particles. The particles dispersed in and passing through the bubble phase play an important role in transferring heat from bubble gas to the bed solids [20]. The resulting heat transfer coefficient between a surface and a gas-solid suspension consists of two additive components; the bed/particle-surface heat transfer and radiation. The radiation contribution rises rapidly with temperature [25]. In this subchapter, first the intra-particle heat transfer, particle convection, is discussed. Next the bed/particle-surface heat transfer coefficient, where the convection mechanisms are lumped together in relation to a surface is examined, with a brief description of the contribution of radiative heat transfer following. Finally the bed-surface and radiative heat transfer coefficients are

used to determine the heat transfer tube area needed to deliver sufficient heat for the calcination process discussed in this work.

5.2.1 Particle convection

Particle convective heat transfer is due to the convective flow of particles from the in-bed region to the region adjacent to the heat transfer surface. There the particles gain heat by thermal conduction and bring the heat along as they move to a colder part of the bed. Particle convection is the principal mode of heat transfer in fine particle systems. Heat transfer between particles and a gas in a fluidized bed may be compared to gas convection from a single, fixed particle, and to as convection from a packed bed of fixed particles. The heat transfer coefficient increases with increasing thermal conductivity, increasing density, and decreasing viscosity of the gas. Particle convection heat transfer is given by the following equation:

$$h_p \equiv \frac{q}{a_p \cdot \left(T_p - T_g\right)} \tag{5.3}$$

Where for spherical particles $a_p = \pi d_p^2$

From experimental analysis it has been shown that the heat transfer coefficient increases with increasing velocity of the gas relative to the particles. It also increases with increasing thermal conductivity, increasing density and decreasing viscosity. The mechanism for heat transfer becomes more complex as the process changes from single particles, to fixed and lastly fluidized beds. In fixed beds, there is the added complication of particle packing and the complex gas flow pattern that results. In fluidized beds further complication of the movement of suspended particles and bubble formation and coalescence.

The magnitude of the heat transfer coefficient between the particles and gas in a bubbling fluidized bed is generally not large. Values of h_p for common applications have been found to be around 1 – 100 W/m^{2}K. However the rate of heat transfer between particles and gas per unit bed volume is extremely high, due to large interfacial surface area. Concerns with the actual rate of heat transfer between particles and gas arise primarily in

situations where one phase or the other is an intense heat source, such as burning particles in a fluidized combustor [20].

5.2.3 Bed surface heat transfer

In order to heat or cool fluidized beds, heat transfer tubes can be inserted into the reactor carrying cooling or heating fluids into the bed. The bed-surface heat transfer coefficient h_w is defined as:

$$h_w = \frac{Q}{a_w \cdot (T_b - T_w)} \tag{5.4}$$

Where a_w is the submerged area, T_w is temperature of the submerged area, T_b is temperature of particle/gas, and Q is the heat transfer rate (W).

Typical of h_w is that it is several times greater than heat transfer coefficient for single-gas convection. It increases steeply as gas velocity exceeds the minimum fluidization velocity, and attains a maximum value at a specific velocity and declines thereafter. The bed-surface heat transfer also decreases with increasing particle size.

In a SE-SMR process, the calcination is carried out at such high temperatures that radiation plays a role in the overall heat transfer coefficient:

$$h = h_w + h_r \tag{5.5}$$

where h_w is the wall heat transfer coefficient and h_r is the heat transfer coefficient due to radiation, which is more closely described in 5.2.3 below.

5.2.3 Radiation

At temperatures lower than 500˚C, the radiant contribution to the total heat transfer has been measured to be less than 15%, and becoming greater than 35% at temperatures higher than 800˚C [21]. The radiant contribution to the heat transfer can be calculated as follows:

$$h_r = \left(\frac{\varepsilon_b \cdot \varepsilon_w}{\varepsilon_w + \varepsilon_b - \varepsilon_w \cdot \varepsilon_b} \right) \cdot \frac{\sigma \cdot (T_2^4 - T_w^4)}{T_2 - T_w} \tag{5.6}$$

Where σ is Stefan-Boltzmann constant ($5{,}67 \cdot 10^{-8}$ W/(m^2 K^4)). ε_w and ε_b are the emissivities of the wall and bed [21].

5.3 Heat exchanger tubes within reactor

One way of delivering heat to the reactor is by installing horizontal tubes within the reactor. In the tubes, methane is burned and a heat transferred from inside to the surface of the tubes. In order to calculate the necessary heat exchanger area, the bed-wall heat transfer coefficient, h_w can be found via Vreedenbergs correlation. Then, equation (5.7) is used to find the necessary heat exchange area.

In order to get an accurate number for h_w, Vreedenbergs correlation for horizontal tubes can be applied:

$$\frac{h_w \cdot D_t}{k_t} = 0.66 \cdot \mathrm{Pr}_g^{0.3} \cdot \left(\frac{\rho_s \cdot (1-\varepsilon)}{\rho_g \cdot \varepsilon} \right)^{0.44} \cdot \mathrm{Re}_D^{0.44} \quad \text{for} \quad \frac{\rho_s}{\rho_g} \cdot \mathrm{Re}_p \leq 2050 \tag{5.7}$$

$$\text{With } \mathrm{Re}_D = \frac{D_t \cdot \rho_g \cdot U}{\mu_g},\ \mathrm{Re}_p = \frac{d_p \cdot \rho_g \cdot U}{\mu_g},\ \mathrm{Pr}_g = \frac{C_{p \cdot g} \cdot \mu_g}{k_t} \tag{5.8 – 5.10}$$

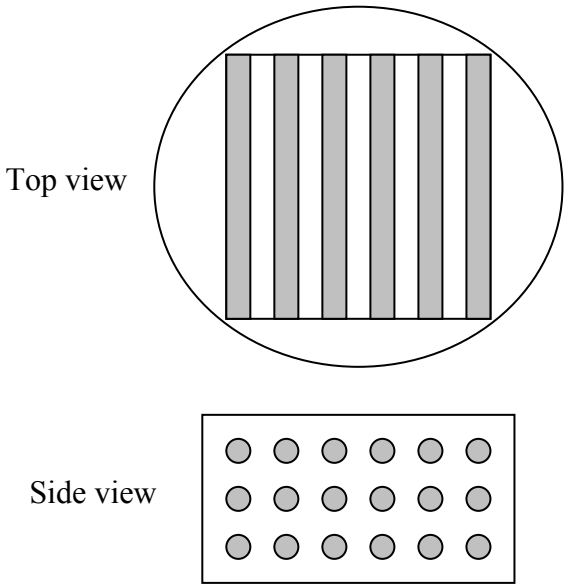

Figure 9: Heat exchanger pipes arrangement in calciner

With u_0 close to u_{mf} the *h* value varies around the horizontal pipe, being lower underneath and above than on the sides. At higher velocities, the values of *h* around the tube are more uniform. With increasing pressure, the fluidization becomes smoother and consequently the *h* value rises. h_w decreases with increasing particle size [21].

In *Appendix C*, a calculation of the heat exchanger area and pipes based on equations (5.5) – (5.10) is included. It is found that with a heating pipe diameter of 8mm and a heat demand of 14.02kW, 12 rows with 8 pipes on each row are needed. The heat demand is calculated in *Appendix E*.

5.4 Heat exchange via in-reactor combustion of biogas

One of the easiest ways of providing enough heat to the fluidized bed, is by direct combustion of gas right above the distributor plate. This way of providing heat has successfully been done at a limestone calciner plant in South Wales, England. The plant has a capacity of 20,000 tonnes per year, and CaO is produced at an energy cost of around 5.5 MJ/kg CaO. Local land fill gas from two land fills is used for providing the necessary heat. The operators report that the relative high levels of CO_2 in the land fill gas does not seem to affect the lime quality [26].

Since for this application, biogas is the initial working medium, it is natural to use it for providing the necessary heat in the calcinator. Part of the work presented here, and the simulation, aims to check if the heating value of the biogas is sufficiently high in order to achieve the desired temperature and have enough energy for the endothermic reaction to be carried out. Calculations of heat capacity and adiabatic flame temperature for different compositions of gas mixtures are given in *Appendix E*. In order to achieve complete combustion of the gas, excess air of 1.1 is usually needed. Too much oxygen will on the other hand have an adverse effect on the catalyst.

5.4.1 Combustion kinetics of methane

With direct burning of methane in the bed, the governing heat transfer will be gas-particle convection between the oxidizing methane and sorbent. In the literature there are many different reaction rate expressions for methane combustion. In natural gas combustion

mechanics, as many as 325 reactions can take place [27]. Instead of setting up all the different reactions that occur, global reactions of methane combustion can be used. Global reactions are derived from curve-fitting, based on a certain range of temperature and stoichiometry. Utilizing global reaction will thus give good results in a limited area, and erroneous values outside of that area. Two global reaction rates examined in this work, but which were abandoned due to modelling complications, are given in *Appendix D*.

For stoichiometric combustion of methane, the enthalpy of combustion reported in literature is [28]:

$$CH_4 + 2(O_2 + 3.76N_2) \Rightarrow CO_2 + 2H_2O + 7.52N_2, \quad \Delta H^\circ_{CH_4} = -802.3\,{}^{kJ}\!/_{mol} \quad (5.11)$$

For this work, excess air of 1.1 will be used.

6 Heat balance without flow considerations

In order to know whether the results from the simulations are within reasonable values, since there are no experimental results, a coarse energy balance based on the desired hydrogen production is made. The hydrogen production, when produced from methane yields a specific CO_2 stream, and in order to absorb all the CO_2, a specific amount of continuous supply of sorbent is needed. For simplicity, the reactor is considered perfectly insulated, i.e. the heat consumed is exclusively used in heating solids and gas. With a hydrogen production of $10Nm^3/h$, and a CO_2 uptake in the sorbent of 22%, the one-dimensional model proposed by Johnsen (2006) yields a solid stream of 0.78 kg/min of calcined dolomite out of the calciner [16].

Calculations on the flow of sorbent and the grade of calcination are given in *Appendix G.*
The heat balance then becomes the following:

Heat from fuel = heat to calcination + heating of CO_2 released in the calcination + heat to sorbent + heat to catalyst

$$Q_{fuel} = Q_{calc}\dot{m}_{calc} + M_{CO_2}Cp_{CO_2}\Delta T + M_{CaCO_3}Cp_{CaCO_3}\Delta T + M_{cat}Cp_{cat}\Delta T \quad (6.1)$$

SNG, or pure methane, CH_4 is used as basis for the calculations, which can be found in *Appendix E*. From the calculations, a heat demand of Q=14.02kW is found. This corresponds to the complete combustion of a methane stream of 0.01746 mol/s.

7 Mathematical model of calcinator

In order to describe the calcination process accurately, a mathematical model of the governing physical regimes is necessary. Simplifications of the problem are made in order to make the modeling process easier. The model described in this chapter is a fixed bed model. A more detailed description of the model itself is given in *Chapter 10*. Basis for the momentum, energy and mass conservation equations are taken from [29].

7.1 Momentum equations:

In describing the bed as fixed, Brinkman, derived from Darcy's law can be applied:

$$0 = -\nabla P + \mu\nabla^2\vec{v} - \mu\kappa^2\vec{v} \qquad \nabla\vec{v} = 0 \tag{7.1}$$

Brinkman is valid for a Reynolds numbers below 10. Testing if valid:

$$\mathrm{Re}_D = \frac{D_t \cdot \rho_g \cdot U}{\mu_g} = \frac{187 \cdot 10^{-6} \cdot 0.309 \cdot 2.4}{4.28 \cdot 10^{-5}} = 3.24 \tag{7.2}$$

The Brinkman equation includes a viscous resistance term in the Darcy equation to account for solid/fluid interface effects. Derivation of Darcy's Law from Navier Stokes law of momentum and derivation of Brinkman from Darcy's Law is found in *Appendix A* and *Appendix B*.

7.2 Energy equation:

$$\overbrace{\rho \cdot C_p \cdot \frac{\partial T}{\partial t}}^{transient} = \dot{Q}_{calcination} - \dot{Q}_{combustion} + \overbrace{k\left(\frac{\partial^2 T}{\partial x^2} + \frac{\partial^2 T}{\partial x^2}\right)}^{conduction} - \overbrace{\rho \cdot C_p \cdot \left(u \cdot \frac{\partial T}{\partial x} + v \cdot \frac{\partial T}{\partial x}\right)}^{convection} \tag{7.3}$$

Assuming steady state, and the transient part is equal to 0:

$$0 = \dot{Q}_{calcination} - \dot{Q}_{combustion} + \overbrace{k\left(\frac{\partial^2 T}{\partial x^2} + \frac{\partial^2 T}{\partial x^2}\right)}^{conduction} - \overbrace{\rho \cdot C_p \cdot \left(u \cdot \frac{\partial T}{\partial x} + v \cdot \frac{\partial T}{\partial x}\right)}^{convection} \quad (7.4)$$

All energy delivered in the process stems from the combustion of SNG or biogas and is used for heating sorbent and providing energy for the calcination reaction and for heating released CO_2.

7.3 Mass balance:

Mass balance calcination:

$$\frac{\partial C_{CaCO_3}}{\partial t} = \dot{m}_{calc} \quad (7.8)$$

The calcination is carried out with a stable flow of new, uncalcinated sorbent.

Calcination rate:

$$R_{calcination} = 1.22 \exp(-4026/T) \cdot (P_{eq} - P_i) \quad (7.9)$$

The calcination rate is derived and explained in *Chapter 3*.

7.4 Initial conditions:

Initial temperature:

$$T(0) = 500^{\circ} C \quad (7.10)$$

The initial temperature of the bed is set to 500˚C, which is the temperature of the sorbent entering from the carbonation reactor. This temperature will however not affect the steady-state operation of the model.

Initial concentration:

$$C_{Combustion\ /\ Fluidizing\ air}(0) = 0\left[mol/m^3\right] \quad (7.11)$$

Initial concentration of the combustion gases in the reactor is set to zero at t = 0.

Initial pressure:

$$P(0) = 1\ bar \tag{7.12}$$

Initial pressure in the reactor is set to 1 bar.

Voidage throughout bed:

$$\varepsilon = 0.5 \tag{7.13}$$

Bed assumed fluidized loosely packed/fluidized through the entire model.

7.5 Boundary conditions:

Reactor assumed perfectly insulated:

$$-k\frac{\partial T}{\partial x}\bigg|_{x=0} = 0 \qquad -k\frac{\partial T}{\partial x}\bigg|_{x=0.2} = 0 \tag{7.14 – 7.15}$$

No heat loss through the vertical sides of the reactor. Heat only enters bottom and leaves top.

Stream of fluidizing air/combustion gas:

$$\frac{\partial C_{\text{Combustion / Fluidizing air}}}{\partial x}\bigg|_{y=0} = 6.33\left[mol/m^2 s\right] \tag{7.16}$$

The combustion gas is used as fluidizing medium. With given dimensions and heat demand, it is sufficiently high.

Temperature of combustion gas:

$$T\big|_{y=0} = T_{ad}{}^{*}\ [\mathrm{K}] \tag{7.17}$$

* Adiabatic combustion temperature calculated for different compositions of fuel gas, given in *Appendix F*.

8 Dimensioning the reactor and possibilities for integration with heat plant.

8.1 Dimensioning plant and determining streams

When dimensioning the reactor it is reasonable to start with the desired output of the process. In the case of HyNor Romerike the output of hydrogen production is planned at 10Nm^3/h.

8.1.1 Sorbent and catalyst streams

In order to produce that amount of hydrogen and capture the CO_2 which is produced, a certain regeneration rate of the sorbent is needed. With continuous H_2 production of 10 Nm^3/h the adjoining CO_2 production from the reforming process will be 2.62 Nm^3/h. The following relation is given for conversion of dolomite [16]:

$$X_{CaO} = \frac{\Delta w(t)}{w_0 \cdot \frac{Y_{CaO}}{Y_{Total}} \cdot \left(\frac{M_{CaCO_3}}{M_{CaO}} - 1 \right)} = \frac{\Delta w(t)}{w_0 \cdot 0.472} \tag{9.1}$$

where X_{CaO} is the conversion factor, $\Delta w(t)$ is the weight increase, w_0 is the initial weight of calcined dolomite, YCaO is the CaO content in the dolomite, $Y_{Total} = Y_{CaO} + Y_{MgO} + Y_{Impurities}$. M_{CaO} and M_{CaCO3} are the molar weights of CaO and $CaCO_3$.

The conversion rate will decrease significantly during initial operation, and stabilize on a certain value. By experiments this value is found to be approximately 22%. The 2.62 Nm^3 or 4.7 kg CO_2 being produced every hour, would be the weight increase, $\Delta w(t)$, which means a total mass of 45.49 kg sorbent is circulated within an hour. Of the total mass, 6.01 kg CaO is regenerated in the calcinator per hour. Sorbent calculations are given in *Appendix E*.

8.1.2 Physical dimensions

The inner diameter of the reactor is 20cm, and a bed height is 50 cm. The fluidization velocity if the reactor uses internal heat tubes for heat transfer is 0.1 m/s, which equals a fluidizing gas stream of 2.70Nm^3 per hour. The combustion exhaust gas, when SNG is used as fuel and regular air is used as oxidizing medium, far exceeds this stream with a total gas stream of 69.46 Nm^3/hr or 2.57 m/s, thus making a separate fluidizing stream unnecessary. With combustion of biogas, this velocity increases to 3.1 m/s.

8.1.3 Energy needed

Energy is needed for heating of the combustion air, heating of the sorbent and catalyst, heat for the calcination reaction, and heating of the released CO_2. In *Appendix D*, a heat balance for the reactor is set up, and it is found that the effect needed is 14.02kW.

8.2 Possibilities of integration with central heating plant

Since the SE-SMR will be located on the same site as a heating plant, the possibility of efficiency benefits due to available high temperature energy should be looked into. First, the reactor needs to reach a temperature of 500˚C to start the reforming process. Then, in order to regenerate the sorbent, 900˚C heat is needed. The first natural way of utilizing the available heat would be to heat the carbonated sorbent, methane and air with the calcinated sorbent and flue gases, but due to irreversible losses it will not be large enough. At the central heating plant, burning of biogas will work as the base load for the plant. In the heating part of the sorbent, there will be little or no gain from using the exhaust gas from the central heating plant burner, as the land fill gas can be used directly in the burner with lower losses to the environment. The sorbent needs however to be cooled to ~500˚C before entering the reformer. Specifically, the heat released in this process would be:

$$Q = \dot{m} \cdot Cp_{sorbent} \cdot \Delta T = 0.013 \cdot 1300 \cdot (900 - 500) = 6760W \qquad (9.2)$$

Also the heat contained in the exhaust gas from the combustion of the biogas can be used down to temperature of the circulating water:

$$Q = (\dot{m}_{flue} \cdot Cp_{flue} + \dot{m}_{CO_2} \cdot Cp_{CO_2})\Delta T = (0.00472 \cdot 1420 + 0.0013 \cdot 1270) \cdot (900 - 80) = 6850W \quad (9.3)$$

In other words, there are theoretically 13.5 kW available heat effect. If the heat effect from 900˚C to 500˚C is used in the process itself, 3.5 kW is left for other purposes.

9 Model Description

9.1 Modelling in COMSOL Multiphysics

COMSOL Multiphysics, formerly known as FEMLAB, is a finite element method modelling program which can be used to model various physical phenomena and engineering applications based on partial differential equations. One of its strengths, as the name Multiphysics implies, is modelling problems where several physical regimes have an effect. COMSOL has an interface to MATLAB, and also its own interface called COMSOL Script. In addition it has an extensive material library. One can also add extra differential equations if wanted [30].

9.2 Fluidized bed models

There are generally two types of approaches to modelling of fluidized beds that have been widely recognized; the pseudo homogeneous approach and the two-phase approach. The pseudo homogeneous approach employs ideal or simple one-parameter models, like plug flow, complete-mixed, dispersion, and tank-in series models. The model has however had problems in accurately describing the conversion of the flow in reactors, and has been modified on terms of residence time distribution, and been altered to compensate for the differences in the emulsion and bubble-phase, but has still not given satisfactory results. Discouraging results with the pseudo homogeneous models have led to an increased focus on two-phase models. The two phase model considers the bed to consist of at least two phases, a dense and a bubble phase. Essentially it states that all the gas in excess of fluidizing the bed passes through as bubbles [16].

9.3 Model Assumptions

COMSOL has not formerly been used for modelling fluidized beds. For the scope of this thesis, considering available time, and the advice from consultations with experts on the field of two-phase modelling and fluidized beds, several simplifications were made in order to develop a model that incorporates combustion of methane and calcination.

Simplifications and assumptions for the model are the following:

1. Fixed bed approximation
2. No bubble formation
3. Steady state modelling
4. Perfect mixing in reactor
5. Isotropic heat transfer
6. In-flow of catalyst and calcite is continuous
7. Catalyst is not separated from sorbent before entering calciner
8. Only the middle cross-section of the reactor is modelled
9. Methane combustion is carried out in a “black box”, flue gas with a given heat capacity and temperature is modelled as the inflow of fluidizing gas.
10. Fluidizing gas stream is uniform over the entire bed, i.e. no jets from distributor plate
11. The reactor is perfectly insulated
12. Thermal conductivity of fluidized bed is double that of fixed

9.4 Setting up the model

9.4.1 Reactor physical dimensions

The first step after the assumptions have been taken is to create a simple, 2D model of the reactor cross section in the COMSOL CAD environment. The reactor modelled has a diameter of 0.2 m and a height of 0.5 m.

9.4.2 Physical regimes

The second step is adding the needed physical regimes for the process which correspond to the mathematical model. For the model of the calciner, physical regimes of momentum/laminar flow, mass transfer/diffusion and convection/conduction will be modelled.

Momentum/flow

The flow through the reactor is set as the mean flow velocity of air through the distributor plate. The only fluidizing medium is the exhaust gas from the combustion of different grades of biogas. The different grades with the corresponding volumetric flows are given in *Appendix E*. Viscosity of the different gaseous mixes are given in *Appendix K*. As for the flow in the bed, the Brinkman equation governing, a porosity of 0.5 is assumed and a permeability of 1e-5, which is the permeability of well sorted gravel [31], as opposed to a permeability of 5.82e-11, which from equation (5.2) is what the permeability would be if the bed was fixed. When SNG is used as fuel gas, the fluidizing gas velocity is 2.57 m/s. With biogas, the gas velocity rises to 3.1 m/s. Calculations of the gas velocities are based upon the base stream of 0.0175 mol/s of methane combusted with 1.1 excess air.

Mass transfer and diffusion for combustion gases:

The products of the methane combustion, O_2, CO_2, H_2O and N_2 are inserted in a diffusion/convection regime, with its corresponding diffusion coefficients. The diffusion coefficients for the combustion products are given in *Appendix J*. Concentrations of the different species from the methane combustion are based upon complete combustion in an excess air, and ideal gas molar content of a 900˚C and 1 atm environment.

Mass transfer and diffusion for calcination:

The species of the calcination, $CaCO_3$, CaO and CO_2 are inserted into another diffusion/convection regime, where the governing reaction rate of calcination is inserted as a rate of reduction of $CaCO_3$ and production of CaO and CO_2. Diffusion coefficients for the diffusion in the sorbent are based upon diffusion inside a porous structure and is given in *Appendix J*. The initial concentration of CaO is set to 0, as it is assumed that the sorbent is fully carbonated as it enters the calciner. The initial concentration of CO_2 for the calcination regime is the same as for the combustion exhaust gas. The initial concentration of $CaCO_3$ on the other hand is determined on flux of the sorbent. With a diameter of 0.2m and a molar stream of 0.126 mol/s of $CaCO_3$, which equals a flux of 4.017 mol/m^{2}s. This again equals an initial concentration of 1.6 mol/m^3 of $CaCO_3$.

Convection/Conduction

Heat is transferred via convection and conduction within the reactor, mainly between gas and particles. Biogas/methane is burned outside the reactor and the exhaust gas is used as fluidizing medium. Calculation of the heat capacities of the different gas compositions are given in *Appendix E*. The initial temperatures of the exhaust gases were found using Fuelsim Average, a spreadsheet developed for combustion calculations, and are given in *Appendix F*. The walls of the reactor are modelled perfectly insulated. The thermal conductivity of the bed is different from a fixed to a fluidized bed. The effective thermal conductivity of a fixed bed is given by equation (5.2) and parameters from [32]. For the fluidized bed model, the effective thermal conductivity is assumed to be the double of the fixed.

Heat balance

Regeneration of the sorbent is input as a convection/conduction heat-sink. The mass transfer rate used is the decomposition rate of $CaCO_3$. Since the decomposition rate is dependent on temperature and CO_2 concentrations in the bed, using this rate might lead to a rate larger or smaller than what is set by the parameters in the sorbent calculations made in *Appendix E*. Heat source inputs are all heat sinks from the calcination reaction, heating of solids and released CO_2 gas. It is important to remember adding the heating of the sorbent as a whole, and not just the part which is calcinated. Heat balance given below:

$$Q = \overbrace{-rate \cdot \Delta H_{calc}}^{Calcination\ reaction} - \overbrace{\dot{m}_{calc} \cdot Cp_{calc} \cdot dT}^{Heating\ of\ sorbent} - \overbrace{\dot{m}_{cat} \cdot Cp_{cat} \cdot dT}^{Heating\ of\ catalyst} - \overbrace{rate \cdot Cp_{CO_2} \cdot dT}^{Heating\ of\ CO_2\ from\ calcinatin} \quad (9.1)$$

9.5 Interpretation of the model

One important factor with establishing a model is to know how to evaluate the results of the model. In this case, the evaluation of the results is based on the specific numbers for regeneration of necessary sorbent stream when a hydrogen production of 10 Nm^3/hr is to be sustained. Firstly, the temperature of the reactor has to be at least 900˚C for the calcination reaction to be carried out properly. Other factors which tell if the calcination process is properly done are the fluxes of $CaCO_3$, CaO and CO_2. Of these fluxes, the flux of CO_2 is chosen as the parameter of verification in this work.

There is already a CO_2 flux into the reactor from the combustion of SNG or biogas outside of the reactor, and a specific flux of CO_2 will emerge from the calcination reaction when it is fully carried out. The flux of CO_2 which is the same as the flux of CaO from equation (2.6) is calculated in *Appendix G*.

10 Model Results

With the implementation of the model described above, results for the bed temperature, flow patterns and species concentrations can be analyzed. First and foremost, the temperature of the bed is one of the most important ones, and to see if the heating value together with the adiabatic combustion temperature of the exhaust gas is high enough to sustain a continuous calcination reaction. A second parameter which is important is to study the degree of calcination achieved. For the sorbent to be fully calcinated, a temperature of 900˚C or more has to be sustained. Two sets of models are examined, one fixed bed and a modified version of the fixed bed, which should resemble a fluidized bed. Also, two different qualities of fuel gas are examined, the first one being SNG, or 100% methane. The other one, called *biogas*, which resembles the land fill gas at Bøler, contains ~48% CH_4, 47% CO_2 and 5% N_2 [33]. What differentiates the fixed bed from the fluidized bed in this model is the permeability; the ability of a gas to percolate through the bed, and the thermal conductivity; the ability to transfer heat. There are other simplifications made to the model in general described in *Chapter 9.3* which further simplifies the fluidized bed modelled here compared to a general fluidized bed model.

Graphical results from the model runs are presented for the testrun of the model, and for model of fixed bed with SNG as fuel gas. The other graphical results for the model runs with biogas and SNG, which display minor differences between one another, are given in *Appendix N*.

10.1 Testrun of model

The first run of the model is of a fixed bed with SNG as fuel gas. The model yields the temperature profile and CO_2 flux given in Figure 10 and Figure 11 below. The initial molar flux of CO_2 with SNG as source is 0.55 mol/m^{2}s. The mean outflux of CO_2 out of the reactor in Figure 11 is 4.32 mol/m^{2}s. In other words 3.77 mol/m^{2}s comes from the calcination process. The mean temperature on the top of the reactor is 1370K. Both the CO_2 flux and the temperature are higher than expected. A

modification of the relationship between inflow of sorbent and the calcination reaction follows in 10.2.

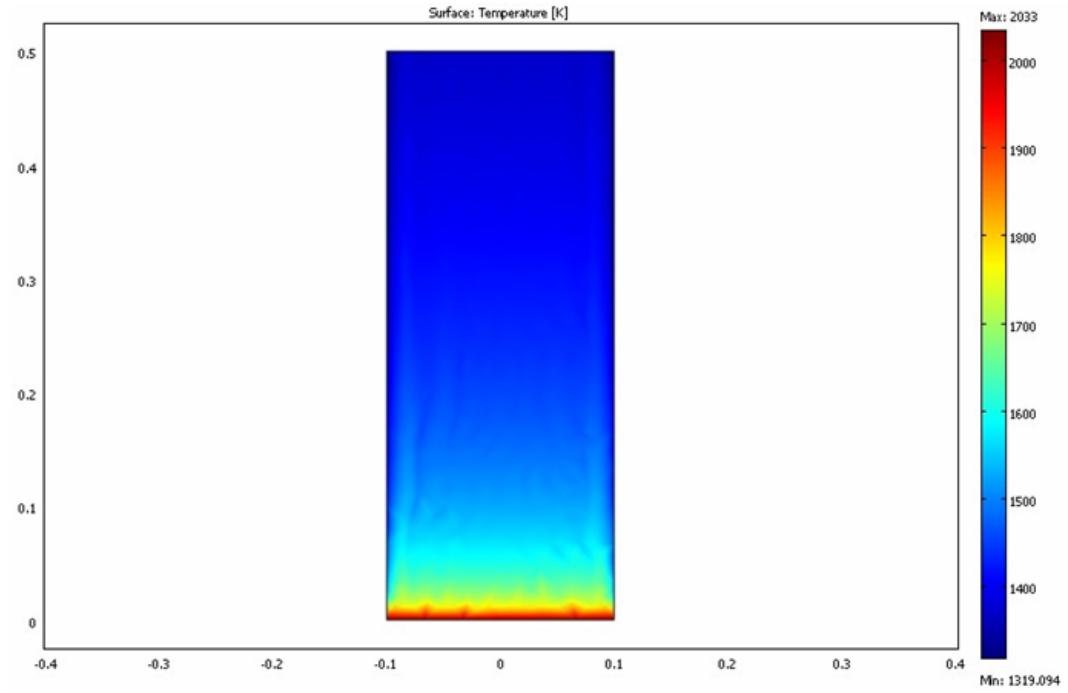

Figure 10: Temperature profile of fixed bed reactor with SNG as fuel gas. Temperature scale given in Kelvin. X and Y-axis are in meter.

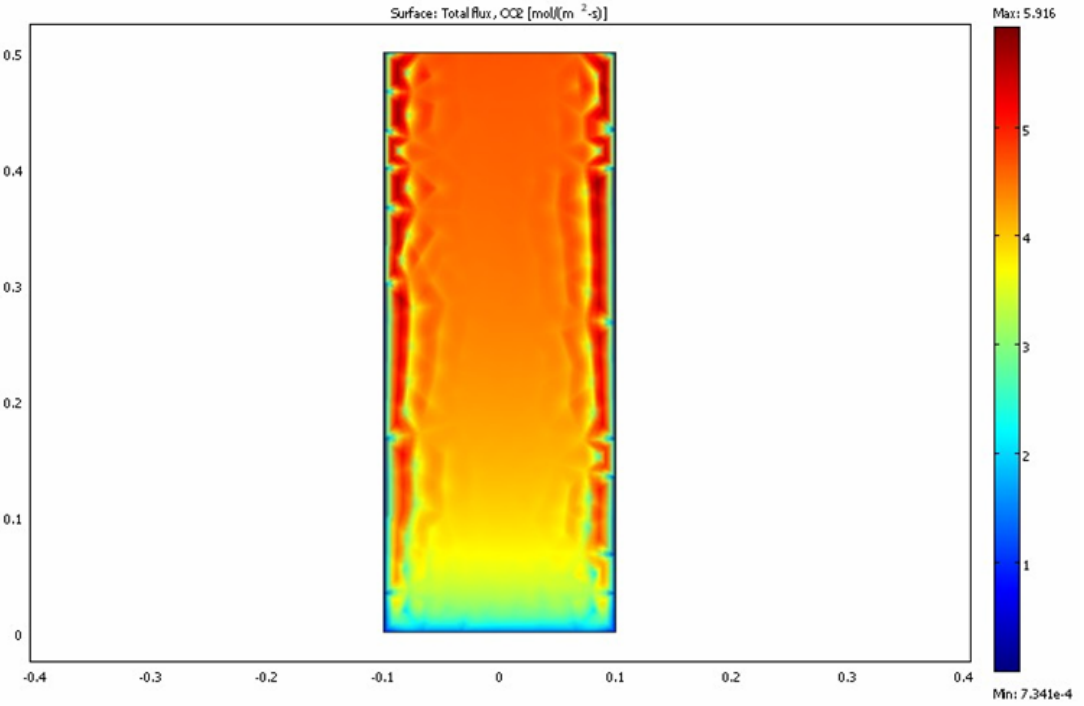

Figure 11: CO_2 flux [mol/m^{2}s] in a fixed bed with SNG as fuel gas.

10.2 Model modification

The calcination process produces 4.7kg CO_2 per hour, or a CO_2 flux of 0.95 mol/m^{2}s. This value is based upon the amount of CO_2 released from sorbent with a H_2 production of 10 Nm^3/hr and is calculated in *Appendix G*. From the initial model results, it is seen that the value of the flux is many times higher than the expected value. One of the reasons for the high conversion rate is the high temperature of the bed. The temperature is directly related to the energy balance given in equation (10.1). In this equation, the inflow of sorbent, $\dot{m}_{calc}$ is a static value, as is the inflow of catalyst, $\dot{m}_{cat}$. One assumption which until now has not been made is full conversion of the sorbent entering the reactor. In order to achieve this in the model, the inflow of sorbent and catalyst must be directly related to the calcination rate. This can be done in the following way:

$$\dot{m}^*_{calc} = \frac{moles\ CaCO_3\ entering\ the\ reactor\ \ per\ hour}{moles\ CaO\ \ produced\ \ per\ hour} \cdot rate = \frac{0.1262}{0.0298} \cdot rate = 4.235 \cdot rate \quad (10.1)$$

The catalyst stream is 35.8% of the stream of sorbent, hence $\dot{m}_{cat}$ becomes:

$$\dot{m}_{cat} = \dot{m}^*_{calc} \cdot 0.358 = 4.235 \cdot 0.358 \cdot rate = 1.52 \cdot rate \quad (10.2)$$

Since the temperature of the bed is dependent on the conversion rate of sorbent and vice verca, a change is made to the expression for the inflow rate of the sorbent. Instead of using a fixed inflow, the inflow is rather directly related to the rate of calcination. This modification leads to another assumption in additions to the ones presented in *Chapter 9.3*: that all the sorbent entering the reactor is calcinated.

10.3 Calcination in a fixed bed

10.3.1 Fixed bed with SNG

With modifications of the relationship between calcination and inflow, the following results are achieved for the fixed bed with SNG as combustion gas. The mean temperature at the top of the reactor shown in Figure 12 is 1218 K, and the mean CO_2 flux shown in Figure 13 is 1.16 mol/m^{2}s, corresponding to a stream of CO_2 from the calcination process of 0.61 mol/m^{2}s, which gives a calcination percentage of 64.21%. From the temperature profile it can be seen that no hot-spots are formed.

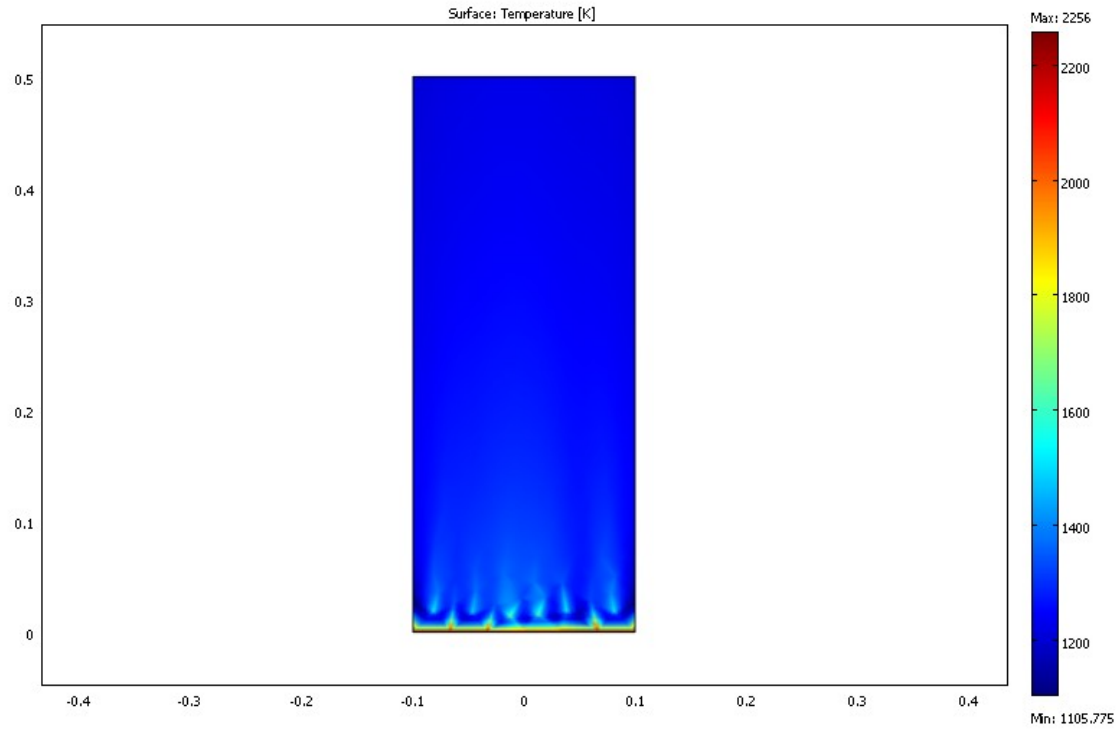

Figure 12: Temperature profile of fixed bed reactor with SNG as fuel gas. Temperature scale given in Kelvin, x and y-axes are in meter.

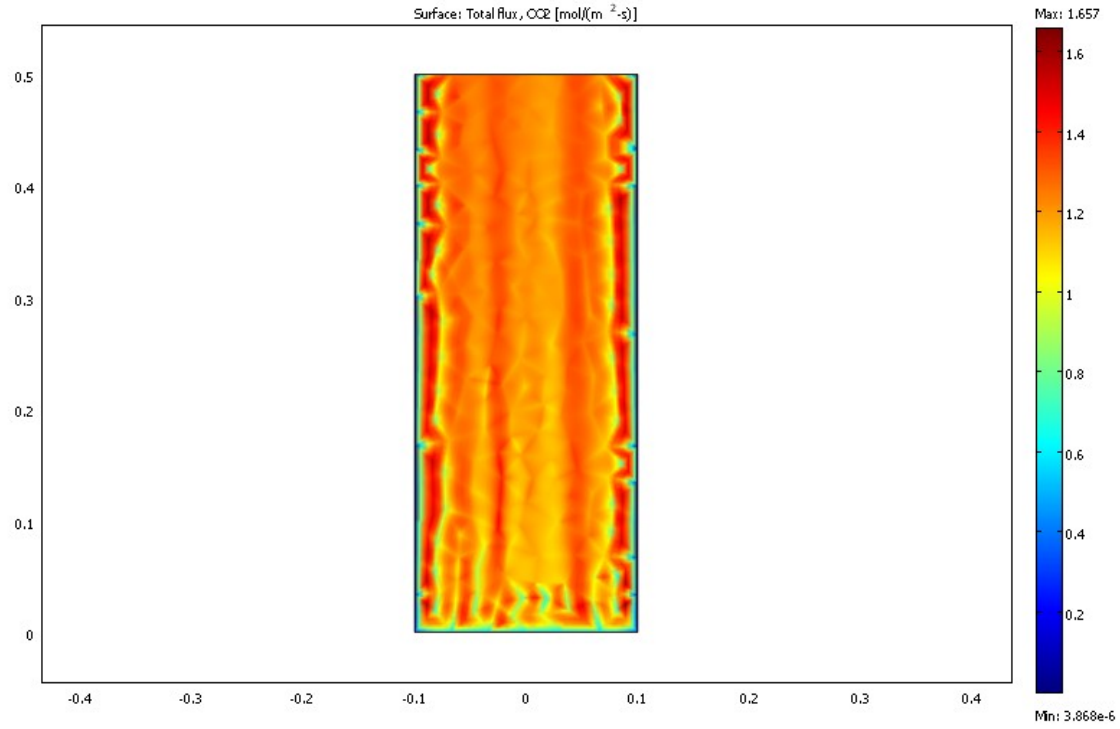

Figure 13: CO_2 flux[mol/m^{2}s] in a fixed bed with biogas as fuel gas, x and y-axes are in meter.

10.3.2 Fixed bed with biogas

Combustion of biogas yields a higher fraction of CO_2 in the exhaust gas, specifically 1.44 mol/m^{2}s. The lower amount of methane in the biogas leads to a lower adiabatic flame temperature, lower heat capacity and some minor changes in gas viscosity and density compared to the 100% CH_4 SNG. It does not however affect the final temperature of the reactor to any big degree. In fact, the mean exit temperature of the reactor is slightly higher than for the SNG. This result is discussed in detail in *Chapter 11.1*. The mean flux of CO_2 at the top of the reactor is 1.95 mol/m^{2}s, which is equal to an increase of 0.51 mol/m^{2}s from the calcination, yielding a calcination percentage of 53.68%. The mean temperature at the top of the reactor is 1248K. Model images of temperature and CO_2 flux are given in *Appendix N.1*.

10.4 Calcination in a fluidized bed

10.4.1 Fluidized bed with SNG

When upgraded biogas, or SNG is burned and sent through the reactor, it yields a mean temperature at the top of the reactor of 1223K. Initial flux of CO_2 is 0.55 mol/m^2s, while the mean flux of CO_2 at the top of the reactor is 1.29 mol/m^2s. A CO_2 flux of 0.74 mol/m^2s thus comes from calcination, yielding a calcination percentage of 77.89%. Model images of temperature and CO_2 flux are given in *Appendix N.2*.

10.4.2 Fluidized bed with biogas

The composition in the biogas is as described 10.3.2. The mean temperature at the top of the bed is 1248K. The initial flux of CO_2 is 1.44 mol/m^2s. The CO_2 flux at the top of the bed is 2.08 mol/m^2s. Flux of CO_2 due to calcination is then 0.64 mol/m^2s, yielding a calcination percentage of 67.37%. Model images of temperature and CO_2 flux are given in *Appendix N.3*.

10.5 Model comments

10.5.1 Determining mean values at top of the reactor

The values for temperature and different fluxes in the reactor vary depending on the location of the reactor is activated. For analysis, mean values of the temperature and flux are important. The way to achieve these values is to use a function in the postprocessing menu of COMSOL called *Boundary Integration,* and choose the top boundary of the reactor in order to get the temperature at the top or flux out of the reactor.

10.5.2 Grid Refining

One way of getting a more accurate solution from a model is refinement of the finite element grid. In this case, one degree of grid refining of the different models yields a significant difference in the mean results, and eliminates local high maxima and low minima, especially for the flux of CaO and $CaCO_3$. A graphical representation of the difference is shown in Figure 14. At the most, a 21% variation in the results due to

grid refining is found. It also shows that the biogas in general yields 12% less calcination than the SNG.The results of the grid refining are presented in Table 1 below.

Table 1: CO_2 recovered from sorbent, for default(normal) grid and for one degree of grid refining

CO_2 recovered:					
	Molar flux of CO_2[mol/m^2s]		Percentage of ideal [%]		Ref.diff[%]
Reactor config,fuelgas	*normal*	*Grid refining*	*normal*	*Grid refining*	*difference*
Fixed,SNG	0,61	0,69	64,21	72,63	13,11
Fixed,biogas	0,51	0,62	53,68	65,26	21,57
Fluidized, SNG	0,74	0,82	77,89	86,32	10,81
Fluidized, biogas	0,64	0,72	67,37	75,79	12,50

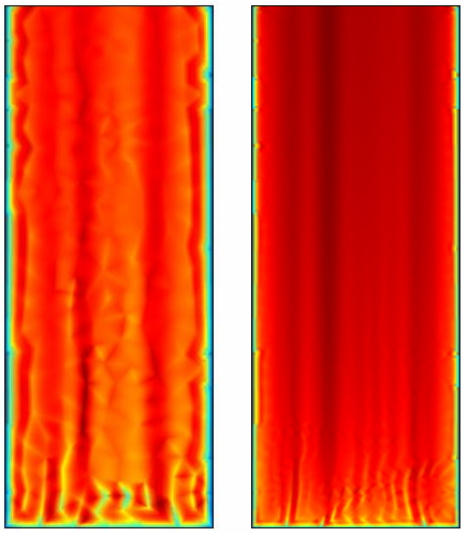

Figure 14: Change in model results for CO_2 flux from default grid to one degree of grid refinement.

10.5.3 Sensitivity Analysis

Eventhough the temperature of the bed is high enough for calcination, it is not fully carried out. In order to see how parameters such as adiabatic flame temperature, heat capacity of the exhaust gas, and thermal conductivity affect the bed, a sensitivity analysis is carried out on the fluidized bed configuration. The results are presented in Table 2 below, where the CO_2 flux is the flux from calcination. Since all the model results are from the SNG case with 100% combustion of methane, there will be an initial flux of CO_2 of 0.55 mol/m^2s. This flux is subtracted in all the results shown in Table 2. The sensitivity analysis is based upon model results with default grid.

Table 2: Sensitivity analysis with *Factor* as the scaling unit.

Sensitivity Analysis						
Factor	T_{ad} *[K]*	CO_2 *flux [mol/m^2·s]*	*Cp [J/kg·K]*	CO_2 *flux [mol/m^2·s]*	*Thermal concuctivity[W/m·K]*	CO_2 *flux [mol/m^2·s]*
1,4	3158	-	1992	0,95	1,75	0,80
1,2	2707	1,26	1708	0,84	1,50	0,77
1,1	2482	0,93	1565	0,79	1,38	0,75
1	2256	0,74	1423	0,74	1,25	0,74
0,9	2030	0,58	1281	0,69	1,13	0,73
0,8	1805	0,42	1138	0,64	1,00	0,71

In Table 3, the CO_2 fluxes are seen in relation to the base case with scaling factor = 1:

Table 3: Relative changes in CO_2 flux

Factor	T_{ad}	*Cp*	*Therm.cond*
1,4	-	1,28	1,08
1,2	1,70	1,14	1,04
1,1	1,25	1,07	1,02
1	1,00	1,00	1,00
0,9	0,79	0,93	0,98
0,8	0,56	0,86	0,96

From the sensitivity analysis it is seen that the temperature of the bed, and the heat capacity are the strongest factors, while a change in thermal conductivity from the initial value does not have a big effect on the calcination.

11 Conclusions and recommendations for further work

11.1 Heat exchanger tubes in a fluidized bed reactor

One way of supplying the heat without disturbing the gases involved in the calcination process is installing heat exchanger tubes in the reactor. Calculations based on Vreedenbergs correlation for horizontal tubes and heat transfer due to radiation demanded an effect of 14.02 kW. This equates to a heat exchanger area of 0.325 m^2 and 96 tubes in 12 rows of 8 tubes, demanding a 0.26m height of the heat exchanger in the bed.

11.2 Discussion of model results

From the temperature profiles with both methane and biogas combustion it seems that the heat supplied is sufficient for both heating of the solids and carrying out the calcination reaction. It is however important to keep in mind the simplifications made in *Chapter 9*, and the residence time of the heating gas in the reactor. The model results however show a calcination rate from 65 – 83% of the ideal. The sensitivity analysis in 10.5.3 points to some factors that can affect the calcination. With increased combustion temperature or increased heat capacity of the gas through the bed, the calcination rate rises and eventually reaches the expected rate. Also an increased heat capacity or thermal conductivity raises the level of calcination.

11.2.1 Temperature profile similarities

The small deviation in temperature of the two configurations described in *Chapter 10*, and the higher temperature of the second configuration with biogas as fuel can to some extent be explained by the lower heat capacity of the biogas. In order for the combustion of biogas to yield the same amount of energy as the SNG, the volumetric flow of exhaust gas is larger, hence the residence time of the exhaust gas molecules is less, giving less time for heat exchange between exhaust gas and sorbent. A higher volumetric flow with a gas of lower heat capacity leads to a lower heat exchange with the sorbent, thus increasing the temperature out of the bed. A look at the fluxes of

CO_2 of the two fuel gases show that the sorbent conversion is about 14% and 11% lower in the bed where biogas is used as fuel compared to the case where SNG is used. The lowered conversion rate is an expected result due to the above-mentioned factors.

11.2.2 Similarities between the fixed and fluidized bed model

Due to all the simplifications made in *Chapter 9.3*, in the end only two parameters differed the fixed from the fluidized bed, namely the permeability of the bed and the effective thermal conductivity. The results from the two different models are thus as expected, a little higher for the fluidized bed, but still minor results, both concentration and temperature-wise.

11.2.3 Possibilities of heat integration

An integration with other heat appliances, such as the heating plant where the planned reformer will be located, was looked at in *Chapter 8.2*, and by the results from the calculations done there, the available heat in the process is best used by heating solids and gases used in the SE-SMR process itself, with only a theoretically available 3.5 kW of heat with the production capacity in this work. On a bigger scale, more heat would be available, and it might be used in heat echanging with for example water in a central heating plant.

11.3 Recommendations for future work

Establishing a model which incorporates fluidization

In order to get more accurate results in the modeling process, establishing a model which fully incorporates the hydrodynamics of a fluidized bed, such as bubble formation, coalescence and breakage would be desirable, but would need a larger time frame or previous in-depth knowledge to different models of fluidization and/or knowledge of suitable programs for modeling fludization. Other modeling programs might prove themselves more adequate for the specific task described in this work. A source code for modeling fluid-solid systems called “MFIX” has been written for

FORTRAN, and might prove itself a good candidate for continuing the modeling presented here.

Modeling combustion reactions

With the model established in this work, it is seen that the temperature of the exhaust gas of combustion is sufficient for calcinating the amount required for the given regeneration rate. However, in order to get a more accurate picture of the methane combustion and its effect on fluidizing patterns, the reaction kinetics of methane combustion should be included in future models. Burning the methane in the reactor would lead to higher local temperatures and fuel could thus be saved.

Modeling the calciner coupled with the carbonator

In order to give an overview over the entire process, a full model with two bubbling fluidized beds coupled together, one working as carbonator/hydrogen production unit, and the other as the calcinator would be desirable. This would however require an extensive amount of time.

References

[1] Dagens Næringsliv, online financial newspaper, http://www.dn.no/, accessed june 2008.

[2] Energy Information Administration, *International Energy Outlook 2007*, http://www.eia.doe.gov/oiaf/ieo/highlights.html

[3] **Rocky Mountain Institute**, "Why Hydrogen", http://www.rmi.org/sitepages/pid203.php, accessed june 2008

[4] **World Resources Institute**, *Global Food Prices Rise to New Heights*, http://earthtrends.wri.org/updates/node/292

[5] **KanEnergi**, *Biodrivstoff – potensial for ny næringsvirksomhet*, 2005

[6] **College of the Desert, Palm Desert, CA, USA,** *Hydrogen Fuel Cell Engines and Related Technologies – Chapter 4,* 2001, http://www1.eere.energy.gov/hydrogenandfuelcells/tech_validation/pdfs/fcm04r0.pdf

[7] **Toyota News Release**, *Toyota Develops Advanced Fuel Cell Hybrid Vehicle,* http://www.toyota.co.jp/en/news/08/0606_2.html, accessed june 2008

[8] **Green Car Congress**, *3M Fuel Cell MEA In Operation More than 7,300 Hours, Beating DOE 2015 Target,* http://www.greencarcongress.com/2008/06/3m-fuel-cell-me.html - more, accessed june 2008

[9] **Holland, G.B., Provenzano, J.J.,** *The Hydrogen Age; empowering a clean-energy future,* Gibbs Smith, 2008

[10] HyNor homepages, http://www.hynor.no/, accessed april 2008

[11] **Simonsen, B.,** *Hydrogen from Biomas at HyNor Junction Romerike*, 2007

[12] **Ulleberg, Ø., Eriksen,. D.E.,** *HyNor-node Romerike forstudie, Utredning av Tekniske konsepter,* 2007

[13] **Barelli, L., Bidini, G., Gallorini, F., Servili, S.,** *Hydrogen production through sorption-enhanced steam methane reforming and membrane technology: A review*, Department of Industrial Engineering, University of Perugia, 2007

[14] **Adams, W.A., Blair, J., Bullock, K.R, Gardner, C.L.,** *Enhancement of the performance and reliability of CO poisoned PEM fuel cells*, Journal of Power Sources 145, 2005

[15] **Chen, Z., Po, F., Grace, J.R., Jim Lim, C., Elnashaie, S., Mahecha-Botero, A., Rakib, M., Shirasaki, Y., Yasuda, I.,** *Sorbent-enhanced/membrane-assisted steam-methane reforming,* Chemical Engineering Science 63, 2008

[16] **Johnsen, K.,** *Sorption-Enhanced Steam Methane Reforming in Fluidized Bed Reactors,* 2006.

[17] *Calcination*, Wikipedia article, http://en.wikipedia.org/wiki/Calcination, accessed may 2008

[18] **Johnsen, K., Meyer, J.,** *Investigation of Sorption Enhanced Hydrogen Production in Fluidized Bed Reactors*, Presentation at Nordic Hydrogen Seminar 2006, http://h2seminar2006.ife.no

[19] **Gilot, P., Stanmore, B.R.**, *Review - calcination and carbonation of limestone during thermal cycling for CO_2 sequestration,* Fuel Processing Technology 86, 2005

[20] **Kunii, D., Levenspiel, O.,** *Fluidization Engineering*, Butterworth-Heinemann, 1991

[21] **Yang, W. C.,** *Handbook of Fluidization and Fluid-particle Systems*, Marcel Dekker, Inc, 2003

[22] **Lide, D. R,** *Diffusion in Gases*, CRC Handbook of Chemistry and Physics, 88th edition, (p. 6-191 and 6-192), , 2008, online version,http://www.hbcpnetbase.com/

[23] **Abba, A.I., Grace, J.R., Bi, H.T.,** Variable-gas-density fluidized bed reactor model for catalytic processes, Chemical Engineering Science 57, 2002.

[24] **Doraiswamy, L.K.,** *Organic Synthesis Engineering, 12. Reactor Design for Solid-Catalyzed Fluid Phase Reactions*, Oxford University Press, 2001

[25] **Chauk, S.S., Fan,L,** *Handbook of Heat Transfer, Chapter 13: Heat Transfer in Packed And Fluidized Beds*, McGraw-Hill, New York,1998.

[26] *Demonstration of a Landfill Gas-Fired Limestone Calciner*,pdf-document,http://ec.europa.eu/energy/res/sectors/doc/bioenergy/aerobic_digestion_composting/09bm_307_91.pdf

[27] GRI-mech 3.0 information, http://www.me.berkeley.edu/gri_mech/

[28] **Yaws, C.L.,** *Enthalpy of Combustion; Organic Compounds*, Chemical Properties Handbook, McGraw-Hill, 1999.

[29] Incropera, F.P., DeWitt, D.P., Fundamentals of Heat and Mass Transfer, Wiley, 2002.

[30] COMSOL Multiphysics, version 3.4, User's guide

[31] **Bear, J.,** *Dynamics of fluids in porous media*, 1972, American Elsevier Publishing Company

[32] **Clauser, C., Huenges,** *Chapter 10: Thermal Conductivity of Rocks and Minerals*, Rock Physics and Phase Relations, Chapter, American Geophysical Union, 1995

[33] **Fossum, T.R.** (tom.roger.fossum@roaf.no), 18.dec 2007. *Gassdata fra ROAF*, E-mail to Simonsen, B. (mailto:bjornsi@stud.ntnu.no)

[34] **Durlofsky, L., Brady, J.F.,** Analysis of the Brinkman equation as a model for flow porous media, Department of Chemical Engineering, California Institute of Technology, 1987

[35] **Meyer, J.,** Excel sheet with heat exchanger calculations, 2008

[36] **Wu, W., Dellenback, P.A., Agarwal, P.K., Haynes Jr., H.W.,** *Combustion of isolated bubbles in an elevated-temperature fluidized be*d, Combustion and Flame 140, 2005.

[37] **van der Vaart, D.R,** *Mathematical Modeling of Methane Combustion in a Fluidized Bed*, Ind. Eng. Chem. Res. 31, 1992.

[38] **Yaws, C.L.,** *Heat Capacity of Gas; Inorganic Compounds (Live Eqns.)*, Chemical Properties Handbook, McGraw-Hill, 1999.

[39] **Skreiberg, Ø.,** *Fuelsim - Average v1.1: A mass, volume and energy balance spreadsheet for continuous combustion applications,* Faculty of Engineering Science and Technology, Institute of Thermal Energy and Hydropower.

[40] **Poling, B.E., Prausnitz, J.M., O'Connell, J.P.,** *11-3 Diffusion coefficients for binary gas systems at low pressures: prediction from theory,* Properties of Gases and Liquids (5th Edition), McGraw-Hill, 2001

[41] **Lydersen, A.L.,** *Fluid Flow and Heat Transfer*. John Wiley and Sons, Chichester, 1979.

[42] **Patil, D. J., Smit, J., van Sint Annaland, M., Kuipers, J. A. M.** *Wall-to-Bed Heat Transfer in Gas–Solid Bubbling Fluidized Beds*, Faculty of Science and Technology, Twente University, 7500 AE, Enschede, The Netherlands, 2005

[43] Snapshot from simulation in Ergun, Ergun 6.0, 2008

Appendix A Derivation of Darcy's Law

Even though Darcy's law was experimentally found independently of Navier Stokes, it can be derived from Navier Stokes' law of momentum:

$$\rho\left(\frac{\partial\vec{v}}{\partial t}+\vec{v}\cdot\nabla\vec{v}\right)=-\nabla p+\mu\nabla^2\vec{v}+\vec{f} \tag{A.1}$$

Where ρ is the density of the fluid, $\frac{\partial\vec{v}}{\partial t}$ is the transient change of the velocity field, $\vec{v}\cdot\nabla\vec{v}$ is the convective acceleration which is the effect of time independent acceleration of the fluid with respect to space, ∇p is the pressure gradient in the fluid, $\mu\nabla^2\vec{v}$ is the effect of viscous shear forces, and $\vec{f}$ is a collective term for other body forces, such as gravity.

First step towards Darcy's law is assuming stationary flow, which cancels out the transient change of velocity, leaving equation a.1:

$$\rho\left(\vec{v}\cdot\nabla\vec{v}\right)=-\nabla p+\mu\nabla^2\vec{v}+\vec{f} \tag{A.2}$$

Secondly, assuming creeping flow since flow in porous media governed by Darcy's law has a low Reynolds number. The result is that the inertia effects can be ignored in comparison to the viscous resistance, i.e. the convective acceleration is cancelled:

$$0=-\nabla p+\mu\nabla^2\vec{v}+\vec{f} \tag{A.3}$$

Thirdly, assuming the viscous resisting force is proportional to the velocity, and opposite in direction yields:

$$0=-\nabla p+\frac{\mu\phi}{\kappa_i}\vec{v}+\vec{f} \tag{A.4}$$

Where ϕ is the porosity, and κ_i is the permeability. With the only body force being gravity, the equation becomes:

$$0=-\nabla p+\frac{\mu\phi}{\kappa_i}\vec{v}+\rho g_x \tag{A.5}$$

Arranged:

$$\vec{v} = \frac{-\kappa_i}{\phi\mu}(\nabla p - \rho g_i) \tag{A.6}$$

$\vec{v}$ is related to the Darcy flux, q, by the porosity ϕ:

$$\vec{v} = \frac{q}{\vec{v}} \tag{A.7}$$

which gives Darcy's Law:

$$q_i = \frac{-\kappa_i}{\mu}(\nabla p - \rho g_i) \tag{A.8}$$

For two dimensions, the effect of gravity can be neglected:

$$q_i = \frac{-\kappa_i}{\mu}\nabla p \tag{A.9}$$

Expressed with pore velocity:

$$0 = -\nabla P + \frac{\mu\phi}{\kappa_i}\vec{v} \tag{A.10}$$

Appendix B Derivation of Brinkman equations from Darcy's Law

Darcy's Law, as derived in *Appendix A* accounts only for flow in porous media and low velocities. Brinkman combined the Stokes Equations which describe flow on a microscale level and Darcy's Law which describes the flow at macroscale:

Darcy's Law:

$$0 = \frac{-\kappa_i}{\phi\mu}\nabla P - \vec{v} \tag{B.1}$$

Stokes flow at low Reynolds numbers:

$$0 = -\nabla p + \mu\nabla^2\vec{v} \tag{B.2}$$

Brinkman equation:

$$0 = -\nabla P + \mu\nabla^2\vec{v} - \mu\kappa^2\vec{v} \tag{B.3}$$

The equation is like Stokes Equation, but unlike Darcy's Law second order. This has the significance of allowing for the solution of flow around a particle or motion caused by a particle with no-slip boundary conditions on the surface [34].

Appendix C Heat exchanger calculations

Heat exchanger tube calculations based on [16] and [35]

Calciner properties

Inner diameter, Di	0,2	m
Temperature, T	900	°C
Fluidizing air, U	0,1	m/s
Permeability, κ	2,3E-10	m^2
Effect, Q	14,02	kW

Heat exchanger, physical properties

HEX area, aw	0,325	m^2
Quadratic area:	0,14	x0,14
Areal, one tube, At	0,0035	m^2
Number of tubes, Nt	92,507	
Tube spacing per row	17,5	
Tubes per row, theoretical	8,75	
Tubes per row	8	
Rows, theoretical	11,5633	
Rows, theoretical	12	
Rowspacing	0,01086	m
HEX height	0,26057	m

Heat transfer parameters

HEX Tube diameter, D_t	0,008	m
Particle diameter, dp	1,87E-04	m
Solids density, ρ_s	1724	kg/m^3
Gas density, ρ_g	0,3887	kg/m^3
Gas viscosity, μ_g	4,39E-05	Pa.s
Gas heat capacity, $C_{p,g}$	1795	J/kg.K
Gas thermal conductivity, $k_{t,g}$	0,0961	W/m.K
Bed voidage, ε	0,5	
Re_D	7,08E+00	
Re_p	1,66E-01	
Pr_g	0,8199844	
hw, from Vreedenbergs corr	0,707	kW/m^2K

Wall temperature, Tw	950	°C
Bed emissivity, e_b	0,9	
Wall emissivity, e_w	0,95	
Stephan Boltzman const	5,67E-08	$W/(m^2K^4)$
Radiative heat transfer coeff, hr	0,1543577	kW/m^2K
Total heat transfer coeff, h	0,861	kW/m^2K

Vreedenbergs correlation

$$\frac{h_w \cdot D_t}{k_t} = 0.66 \cdot \mathrm{Pr}_g^{0.3} \cdot \left(\frac{\rho_s \cdot (1-\varepsilon)}{\rho_g \cdot \varepsilon} \right)^{0.44} \cdot \mathrm{Re}_D^{0.44}$$

$$\mathrm{Re}_D = \frac{D_t \cdot \rho_g \cdot U}{\mu_g} \qquad \mathrm{Re}_p = \frac{d_p \cdot \rho_g \cdot U}{\mu_g} \qquad \mathrm{Pr}_g = \frac{C_{p,g} \cdot \mu_g}{k_t}$$

Radiative heat transfer coefficient

$$h_r = \left(\frac{\varepsilon_b \cdot \varepsilon_w}{\varepsilon_w + \varepsilon_b - \varepsilon_w \cdot \varepsilon_b} \right) \cdot \frac{\sigma \cdot \left(T_2^4 - T_w^4 \right)}{T_2 - T_w}$$

Heat transfer coefficient

$$h = \frac{Q}{a_w \cdot (T_w - T_2)}$$

Appendix D Methane combustion

Methane combustion in air is a very fast reaction and involves many elementary reactions before the final products of the combustion are achieved. Global, curve-fitted reactions for methane combustion within a limited range of temperature and stoichiometry are however useful, as long as the case at hand is within that range. Two reaction rates have been studied and efforts were made to implement them in the COMSOL model discussed in this thesis. Problems with non-converging solutions lead however to a simplification of the model, described in *Chapter 7*. Wu et al. [36] present a range of methane combustion rates, one of which was originally proposed by Dryer-Grassman, and is valid for 830 ˚C < T < 1130 ˚C:

$$\frac{d[CH_4]}{dt} = r1 = -10^{13} \exp\left(-\frac{49600}{RT}\right)[CH_4]^{0.7}[O_2]^{0.8}\left(\frac{P}{RT}\right)^{1.5} \quad \text{(D.1)}$$

Another global reaction rate expression which was evaluated and attempted implemented in the model, is one presented in [37]:

$$\frac{d[CH_4]}{dt} = -5.74 \cdot 10^{10}[CH_4]^{-0.5}[O_2]^{1.5} e^{-60000/R_g T} \quad \text{(D.2)}$$

Common for both these reactions is a very high value for *k*, which is to say they are both very fast reactions.

Appendix E Energy balance and heat capacity calculations

Calculation of specific heats from [38].

Energy balance			
species	stream [kg/hr]	Energy [kJ/hr]	Effect [kW]
Heating of $CaCO_3$	45,49	21254,83	5,90
CO2 from calcination	4,72	2186,16	0,61
CaO from calcination	6,01	19103,21	5,31
Catalyst	16,81	7930,57	2,20
Total:		50474,78	14,02

Coefficients for calculation of specific heat (300-1000K)				
Compound	A [J/mol]	B [J/mol^2]	C [JK/mol]	D [J/mol*K^3]
CH4	2,23	9,69E-02	6,11E+05	-2,60E-05
CO	25,87	6,51E-03	1,11E+05	1,02E-06
CO2	29,31	4,00E-02	-2,48E+05	-1,48E-05
H2	25,86	4,84E-03	1,58E+05	-3,70E-07
H2O	28,41	1,25E-02	1,28E+05	3,60E-07
CaO	57,76	-1,08E-02	-1,15E+06	5,23E-06
CaCO3	99,54	2,71E-02	-2,15E+06	2,00E-09
MgO	47,49	4,65E-03	-1,03E+06	-2,70E-07
MgCO3	73,35	6,40E-02	-1,45E+06	2,00E-08
MgAl2O4	153,85	2,68E-02	-4,06E+06	0,00E+00
N2	29,342	-3,54E-03	1,01E-05	-4,13E-09 2,59E-13
O2	3,626	-1,88E-03	7,06E-06	-6,76E-09 2,16E-12

T_{in} [C]	500
T_{in} [K]	773
$T_{calcination}$ [C]	900
$T_{calcination}$ [K]	1173
T_{diff}	400

On calculation of specific heats:

Calculation of specific heat based upon equation below. A temperature between 300 and 1000K is chosen in the blue field above.

$$C_{p,i} = A_i + B_i \cdot T + \frac{C_i}{T^2} + D_i \cdot T^2$$

For calculation of heat capacity of N2 and O2:

$$\frac{\bar{c}_p}{R} = \alpha + \beta \cdot T + \gamma \cdot T^2 + \delta \cdot T^3 + \varepsilon \cdot T^4$$

Calculation of specific heats (300 - 1000K)			
At:	773 K		
	J/(mol*K)	MW(kg/kmol)	kJ/(kg*K)
Air	30,94	28,97	1,068
CH4	62,63	16,04	3,90
CO	31,70	28,01	1,13
CO2	50,96	44,01	1,16
H2	29,64	2,02	14,68
H2O	38,49	18,02	2,14
CaO	50,63	56	0,90
CaCO3	116,93	100,1	1,17
MgO	49,19	40,3	1,22
MgCO3	120,37	84,31	1,43
MgAl2O4	167,80	142,27	1,18
Comb gas:	35,99	27,62	1,30
N2	30,81	28	1,10
O2	33,55	32	1,05

Combustion gas				
species	%	mass (g/m^3)		
N2	0	0	p	101325
CO2	50	228,628282	T	900
H2O	50	93,6123982	Tk	1173
			V	1
			R	8,314
Total	100	322,24068	n (mol/m^3)	10,389833

Specifications of different combustion gases												
	%CH4	%CO2	%N2	mol CO2	mol H2O	mol N2	mol O2	total:	mol CO2	mol H2O	mol N2	mol O2
SNG	1	0	0	1	2	8,27	0,2	11,272	0,92	1,84	7,62	0,18
Biogas	0,48	0,47	0,05	3,083	2	8,38	0,2	13,46	2,38	1,54	6,47	0,18

	Cp (J/mol*K)	Cp (J/kg*K)	ρ(kg/m^3)	Tad, (K)	U (m/s)	mfr. CO2	mfr. H2O	mfr. N2	mfr. O2
SNG	35	1308	0,293	2256	2,57	0,09	0,18	0,73	0,02
Biogas	37	1283	0,319	2033	3,1	0,23	0,15	0,62	0,01

Fluxes of gases [mol/s]					
	U[m/s]	CO2	H2O	N2	O2
SNG	2,57	0,017461701	0,034923403	0,144443	0,0017
Biogas	3,1	0,045085006	0,02924749	0,122491	0,0015

Flux of gases [mol/m^2*s]					
	U[m/s]	A[m^2]	CO2	H2O	N2	O2
SNG	2,57	0,0314	0,56	1,11	4,60	0,06
Biogas	3,1	0,0314	1,44	0,93	3,90	0,05

Burning rate, methane:		
HHV	802900	J/mol
Effect	14020	W/s
Stream, CH4	0,01746	mol/s
Total stream	0,21843	mol/s

Appendix F Adiabatic flame temperature calculations

Fuelsim – Average is a spreadsheet developed for combustion calculations. It is developed by Øyvind Skreiberg at the Institute of Thermal Energy and Hydropower at NTNU.

It is a relatively simple, but useful, mass, volume and energy balance spreadsheet for continuous combustion applications, but can also be used for other thermal conversion processes where solid fuel is converted to a fuel gas mixture of O_2, CO, NO, NO2, UHC (unburned hydrocarbons), SO_2, N_2O, H_2, NH_3, HCN, Tar, CO_2, N_2, Ar and H_2O. The fuel can either be a solid fuel, a liquid fuel or a fuel gas, and the oxidant can either be ISO 2533 Standard air, with a user defined relative humidity, or a gas mixture of O_2 (the only oxidant), N_2, CO_2, Ar and H_2O [39].

For calculations of adiabatic flame temperature from different gas compositions, molar fractions of the different compositions are input in the sheet "Gas Conversions", and are then copied onto the calculation spreadsheet called "Average". Temperatures for the preheating of combustion air and fuel are chosen. Also the amount of excess air in the combustion is chosen. Based upon the mentioned inputs, the adiabatic flame temperature is given.

Appendix G Sorbent calculations

Sorbent calculations based upon works of [16].

Gas properties:		
pressure	101325	Pa
Temperature	298	K
Volume	1	m^3
gas constant	8,314	J/molK
moles	40,8968942	mol/m^3

H2 and CO2 production:

$$CH_4 + 2H_2O \leftrightarrow CO_2 + 4H_2$$

species	MW	Nm^3/hr	mol/hr	mol/s	kg/hr
H2	2,02	10	408,9689	0,1136025	0,826117
CH4	16,04	2,624671916	107,3409	0,0298169	1,721749
CO2	44,01	2,624671916	107,3409	0,0298169	4,724074

Sorbent conversion

$$X_{CaO} = \frac{\Delta w(t)}{w_0 \cdot \frac{Y_{CaO}}{Y_{Total}} \cdot \left(\frac{M_{CaCO}}{M_{CaO}} - 1\right)} = \frac{\Delta w(t)}{w_0 \cdot 0.472}$$

Y_{CaO}	32	wt%
Y_{MgOe}	20,3	wt%
$Y_{impurities}$	1	wt%
X_{CaO}	0,22	
M_{CaO}	56	kg/kmol
M_{CaCO3}	100,1	kg/kmol
Δw(t)	4,72407432	kg/hr
w0	45,4937819	kg CaCO3 / hr
Sorbent flow	0,01263716	kg/s
Sorbent flow	0,12624537	mol/s
Sorbent flow	4,01863349	mol/m^2s
CaO/CO2 flow	0,94913019	mol/m^2s
CaO /hr	6,01109206	kg/hr

Catalyst properties		
Mcat	0,14226	kg/mol
Catalyst stream	0,28	kg/min
Catalyst stream	0,0047	kg/s
Molar stream	0,0328	mol/s
Cp at 1173K	182,38	J/mol*K

Calcination yield per unit fuel:		
Effect:	14,02	kW
Per kg:	2,332355	kW/kg
Per mol:	130,6119	W/mol

Appendix H Revisions and Modeling complications

H.1 Revisions of the model

Initially a fully fluidized bed with in-reactor methane combustion was planned modelled. The process of modelling a fluidized bed involves solving two Navier Stokes equations (one for solid phase and one for gas phase) with different pressure gradients simultaneously, and including bubble formation, coalescence and breakage. There are also many different mathematical models for fluidized beds, and considerable time was initially spent on finding the adequate mathematical model for the process of calcination and methane combustion in a fluidized bed. During this work, I had a conversation with an expert on fluidized bed, Hiromi Takeuchi from the Japanese National Institute of Advanced Industrial Science and Technology, and an expert on two-phase modelling, Terje Sira at IFE. Both pointed out that I had a short time-frame for modelling a fully fluidized bed including calcination and methane combustion kinetics. After consulting with my advisors, it was decided that I would model a semi-fixed bed, based upon the Brinkman equations, which would have some of the characteristics of a fluidized bed(perfect mixing and a voidage of 0.5). The initial model I set up in COMSOL included methane combustion kinetics described in *Appendix D*.

H.2 Complications with the methane combustion kinetics

H.2.1 Rate of combustion reaction – solving with "time-step"

The rates of methane oxidizing reaction, given by equations (D.1) and (D.2) are very fast, with k~10^8. With diffusion coefficients of the different involved gases around 2e-5, the model would not run. There are many different solvers in COMSOL, of which the stationary solver is the default. A time step solver may also be used when reactions occur in small time steps. The solver was thus changed to this mode and appropriate values of time scale and time stepping were input. Still the model would not run. In order to get the model to run the diffusivity coefficients of the involved gases were raised to an order of ~10^7. This is, to say the least, very unsatisfactory.

Another cross check on the diffusion coefficients confirmed that the coefficients were indeed as first found, around 2e-5. The global reaction rate of methane combustion has already been used to describe the combustion in fluidized beds, and with initial temperatures of the ones demanded by (D.1), the model still would not converge.

H.2.2 Mixing of gases

In order to combust properly, methane should be well mixed with the reactants. In the first model, a separate stream of methane is injected 5cm above the distributor plate where air is flowing through and mixes in the reactor where the combustion is taking place. This could potentially lead to errors in the modelling parameters as the combustion reaction is dependent on both CH_4 and O_2 concentrations, and initial values of air within the reactor was set to overcome this problem. That however did not change the results. A small change could be achieved by including methane in the gases streaming up through the distributor plate.This resulted in the possibility of lowering the diffusion coefficients to ~10^4, which is significantly lower than without the perfect mixing, but still in the order of 10^9 higher than the calculated values.

H.2.3 Stabilizing techniques

A feature of COMSOL is “Artificial Diffusion”. This is a correction term that can be added to a given convection-dominated problem which will not solve with the default solver due to instabilities. In studied fields these instabilities are represented as big oscillations, and if large enough will prevent the solver from converging. There are thus several stabilization techniques in COMSOL in order to address these problems. This was tried out, but only led to convergence at very low initial temperatures ($T < 350K$) of the bed.

H.2.4 Abandoning modelling of the methane combustion kinetics

As I was trying out the remedies listed above in order to get the model to converge, I suspected that COMSOL might not be an adequate program for that kind of modelling. After consulting COMSOL support with a detailed specification of my problem I got a reply that in order to include combustion in a COMSOL model, it has

to be imported using Chemkin and COMSOL Reaction Engineering Lab, and that COMSOL itself does not have the proper application modes to treat combustion. Considering that what was the most important task in the modelling process was to examine whether the temperature in the reactor would be high enough with heating of solids and calcination reaction, I rather let the methane combustion reaction be carried out in a “black box” outside of the reactor, and the exhaust gas from the combustion flow through the reactor from underneath, working as the fluidizing gas. I then implemented the calcination reaction and checked if the temperature of the bed was still satisfactory.

Appendix I Thesis progress plan

When the frames around the thesis were set early in 2008, a progress plan was set down in order to structure the work from start to delivery date. Most of the background information on the generalities of the technology was already established from a project work in the fall of 2007[11]. As can be seen from progress report below the plan, the actual work deviated a little from the planned.

Progress plan , master thesis - Bjørn Simonsen

Activity/month	February	March	April	May	June	July
Defining the work	01.02 - 02.03					
Excursion, Nepal		02.03 - 27.03				
Learn COMSOL			27.03 - 21.04			
Matlab model			07.04 - 21.04			
Fluidized bed, background			27.03 - 30.04			
Heat exchange, background			27.03 - 30.04			
Write report, background			15.04 - 07.05			
Dimensions, SESMR			21.04 - 07.05			
Simple model				01.05 - 21.05		
Model version 2				15.05 - 07.06		
Discussion model					01.06 -15.06	
Improvement model					07.06 -21.06	
Results, final report					07.06 -15.07	
Delivering thesis						22.jul

February
I spent most of February defining my work, having meetings with my advisors and researcher Julien Meyer. We also had a discussion about what modelling tool I was to use, and we ended upon COMSOL Multiphysics.

March
Most of March I participated on an excursion with other students from NTNU to Nepal. When I got back I started learning COMSOL with help from Thomas Førde.

April
First week of April I was in Athens on a IEA HIA conference as a step-in for my advisor, Øystein Ulleberg. When I got back I continued with COMSOL and set up a preliminary model of the heat exchanger. At the same time I looked up articles on fluidized beds and heat exchange and calcination in fluidized beds in particular. I also looked at a one-dimensional Matlab model of a fluidized bed developed by Kim Johnsen, but concluded with that it would not assist me specifically in my work and thus abandoned it. Considerable amount of time was spent in finding the appropriate equation system for my problem.

May
More time was spent on learning COMSOL and the equation system. In meetings with other researchers and my advisors we concluded that the two-phase fluidized bed modelling would be too much to accomplish within the available amount of time, and simplifications given in *Appendix H* were made. I did the analytical calculations for the heat exchanger tubes, and found sources for calculating the different necessary parameters. The final equation set for my problem was established in mid May, and I

started modelling. I quickly encountered problems with the reaction rates for methane, (also described in *Appendix H*), and spent considerable amount of time verifying that the reaction rates were correct and changing settings in COMSOL to remedy the problem.

June

In the beginning of June I abandoned the methane combustion kinetics, and instead modelled the combustion as a "black box" combustion outside the reactor, using adiabatic flame temperatures and exhaust gas composition in the model, utilizing the exhaust gas as fluidizing medium. Time was spent finding the appropriate parameters for fixed and fluidized beds and the differences between them. Model constantly improved and tested. Calcination kinetics applied.

July

Further improvement of the model, discussion of the results and general work with the report. Sent the report to my advisors in for comments three weeks before delivery date for a review before final delivery of report on July 22nd.

Appendix J Diffusivity coefficients

Binary diffusion coefficients calculated on the basis of [40] and in porous structures from [16].

Diffusivity calculations

Constants		
T	900	Temperature[C]
Tk	1173,15	Temperature[K]
P	101325	Pressure [Pa]
Pbar	1,0133	Pressure bar
τ	5	Tortuosity factor
ε	0,5	Porosity
rav	1,00E-08	Pore radius[m]

Lennard Jones numbers				
species	*MW[kg/kmol]*	*σ*	*ε/k [K]*	*Ωj*
O2	32	3,47	106,7	0,713169
CO2	44,01	3,94	195,2	0,797696
H2O	18,02	2,64	809,1	1,233343
N2	28,01	3,8	71,4	0,674537

Binary diffusion coefficients						
A - B	**M_{A-B}**	**σ_{AB}**	**D_{AB} [m^2/s]**	**ε/k AB [K]**	**T***	**ΩD**
O2 - H2O	23,056	3,054	2,652E-04	293,821	3,993	0,888
O2 - CO2	37,056	3,704	1,638E-04	144,319	8,129	0,771
O2 - N2	29,872	3,633	2,062E-04	87,283	13,441	0,709
CO2 - O2	37,056	3,704	1,638E-04	144,319	8,129	0,771
CO2 - H2O	25,570	3,291	2,013E-04	397,412	2,952	0,957
CO2 - N2	34,233	3,870	1,616E-04	118,056	9,937	0,745
H2O - CO2	25,570	3,291	2,013E-04	397,412	2,952	0,957
H2O - O2	23,056	3,054	2,652E-04	293,821	3,993	0,888
H2O - N2	21,931	3,220	2,557E-04	240,353	4,881	0,850
N2 - H2O	21,931	3,220	2,557E-04	240,353	4,881	0,850
N2 - CO2	34,233	3,870	1,616E-04	118,056	9,937	0,745
N2 - O2	29,872	3,633	2,062E-04	87,283	13,441	0,709

Binary Diffusion coefficients

$$D_{AB} = \frac{0.00266\ T^{3/2}}{p\sqrt{M_{AB}}\sigma_{AB}^2\Omega_D}$$

$$M_{AB} = 2\left[(1/M_A)+(1/M_B)\right]^{-1}$$

$$\Omega_D = 0.88224(kT/\varepsilon)^{-0.73695} + 0.5624$$

$$\sigma_{AB} = 1/2\cdot(\sigma_A+\sigma_B)$$

$$\Omega_D = \frac{A}{(T^*)^B} + \frac{C}{\exp(DT^*)} + \frac{E}{\exp(FT^*)} + \frac{G}{\exp(HT^*)}$$

A	1,0636
B	0,1561
C	0,193
D	0,47635
E	1,03587
F	1,52996
G	1,76474
H	3,89411
T*	kT/eAB

fuel gas	mfr. CO2	mfr. H2O	mfr. N2	mfr. O2
SNG	0,089	0,177	0,734	0,018
Biogas	0,229	0,149	0,622	0,015

O2 - mix		H2O - mix	
SNG	1,793E-04	**SNG**	2,961E-04
Biogas	1,828E-04	**Biogas**	2,756E-04

CO2 - mix		N2 - mix	
methane	1,808E-04	**methane**	7,526E-04
Biogas	2,137E-04	**Biogas**	4,830E-04

Dpore	Dkn	D_{AB}
3,572E-05	5,008E-06	3,522E-04

Diffusion in multicomponent gas mixtures

$$D_{1-mixture} = \frac{1}{y_2'/D_{1-2} + y_3'/D_{1-3} + \ldots + y_n'/D_{1-n}}$$

$$y_n' = \frac{y_n}{y_2+y_3+\ldots+y_n}$$

Diffusion in porous structures

$$D_{pore} = D_{AB+Kn}\cdot\frac{\varepsilon_0}{\tau}$$

$$D_{Kn} = 97\cdot r_{av}\cdot\left(\frac{T}{M_{CO_2}}\right)^{1/2}$$

Appendix K Viscosity Calculations

Viscosity calculations are based upon coefficients and formula given by Lydersen [41].

Viscosity calculations

Compound	bi	Si
CO2	1,50E-06	220
H2O	1,74E-06	626
O2	1,69E-06	126
N2	1,40E-06	108

Viscosity of species i:

$$\mu_i = \frac{b_i \cdot T^{1.5}}{T + S_i}$$

With T = 1173

Compound	μ	MW	xi_{SNG}	xi_{biogas}
CO2	4,326E-05	44,01	0,088715	0,22908231
H2O	3,886E-05	16,01	0,174338	0,14859393
N2	4,391E-05	28,1	0,655509	0,62232376
O2	5,227E-05	32	0,081438	0,01485939
μ_{SNG}	4,365E-05			
μ_{biogas}	4,378E-05			

Appendix L Geldart classification of particles

By carefully observing fluidization of all sorts of sizes of solids, Geldart (1973) classified the behaviour of fluidized solids into four distinct categories by the density difference between the particles and the fluidizing medium ($\rho_p - \rho_f$), and by the mean particle size, d_p in four categories: C, A, B and D:

Category C:
The bed particles are cohesive and difficult to fluidize, due to interparticle forces being greater than those resulting from the action of the gas. Face powder, flour and starch are typical examples of these solids.

Category A:
The bed particles exhibit dense phase expansion after minimum fluidization and before the beginning of bubbling. Gas bubbles appear at the minimum bubbling velocity, and exhibit controlled bubbling with small bubbles at higher velocities. Particles have a small mean size and/or low particle density ($< \sim 1.4 g/cm^3$)

Category B:
Gas bubbles appear at the minimum fluidization velocity. Sand like particles of sizes typically between 40 and 500μm and density between 1.4 and 4 g/cm^3. At higher velocities bubbles grow large.

Category D:
Stable spouted beds can be easily formed in this group of powders. These particles are either large and/or dense. Deep beds are difficult to fluidize.

In **Error! Reference source not found.**, a graphic of the classification is given, with the calcite marked as a red dot in the category B.

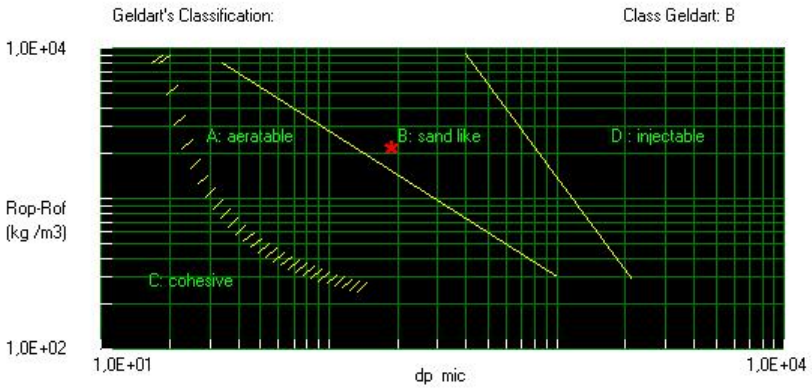

Figure L.1: Geldart classification of particles with dolomite marked off as red dot [42]

Appendix M Model graphics

M.1 Fixed bed with biogas

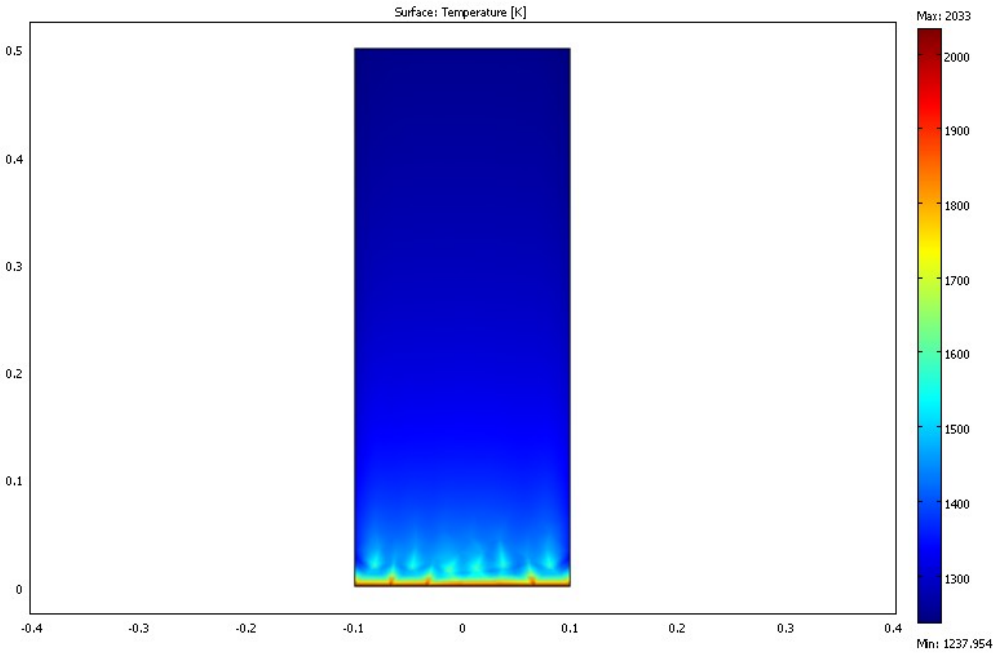

Figure M.1: Temperature profile in a fixed bed with biogas as fuel

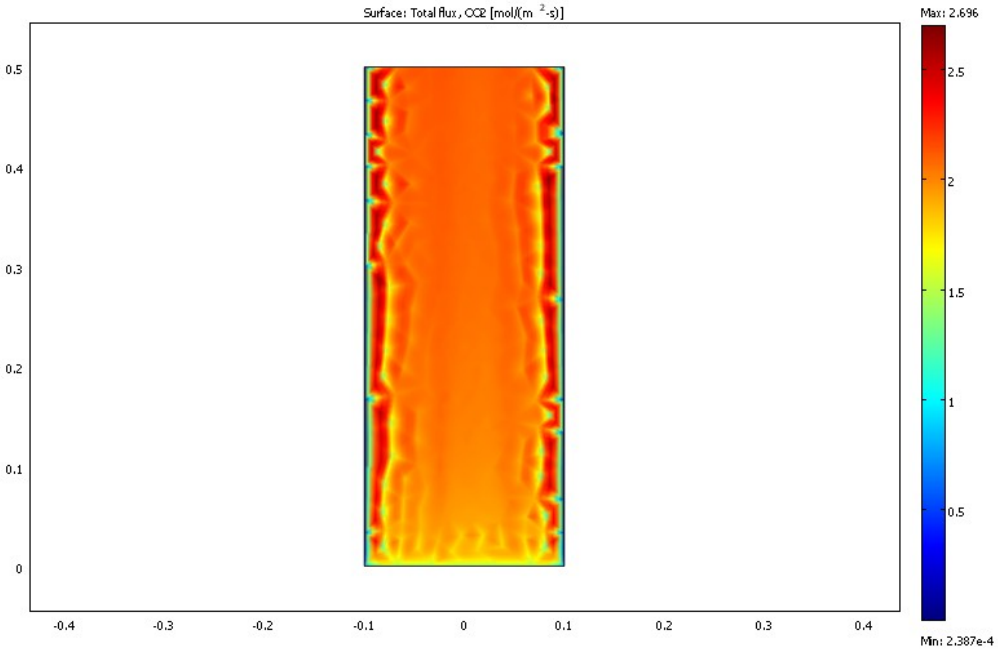

Figure M.2: CO_2 flux in a fixed bed with biogas as fuel

M.2 Fluidized bed with SNG

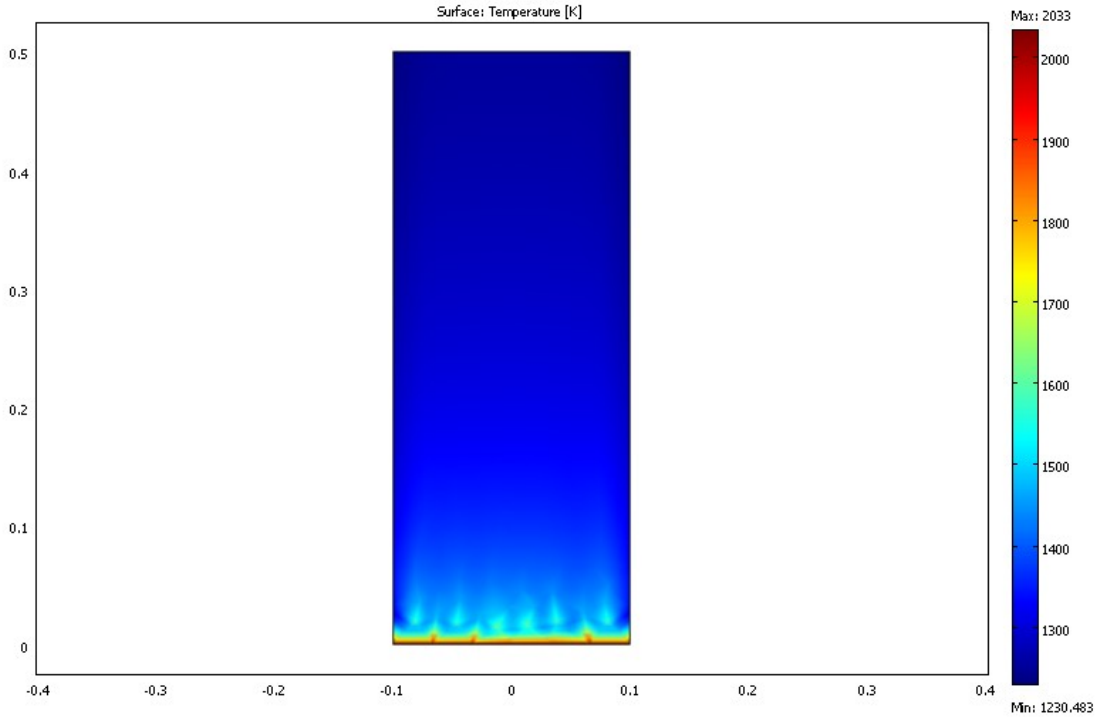

Figure M.3: Temperature profile in a fluidized bed with SNG as fuel

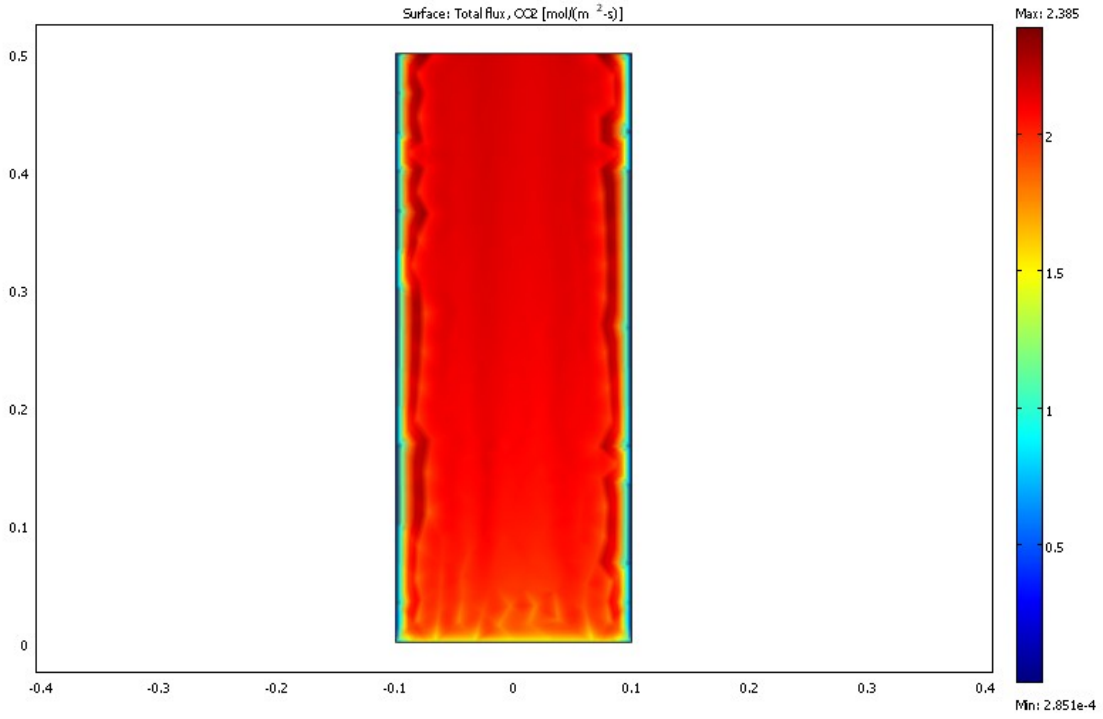

Figure M.4: CO_2 flux in a fluidized bed with SNG as fuel

M.3 Fluidized bed with biogas

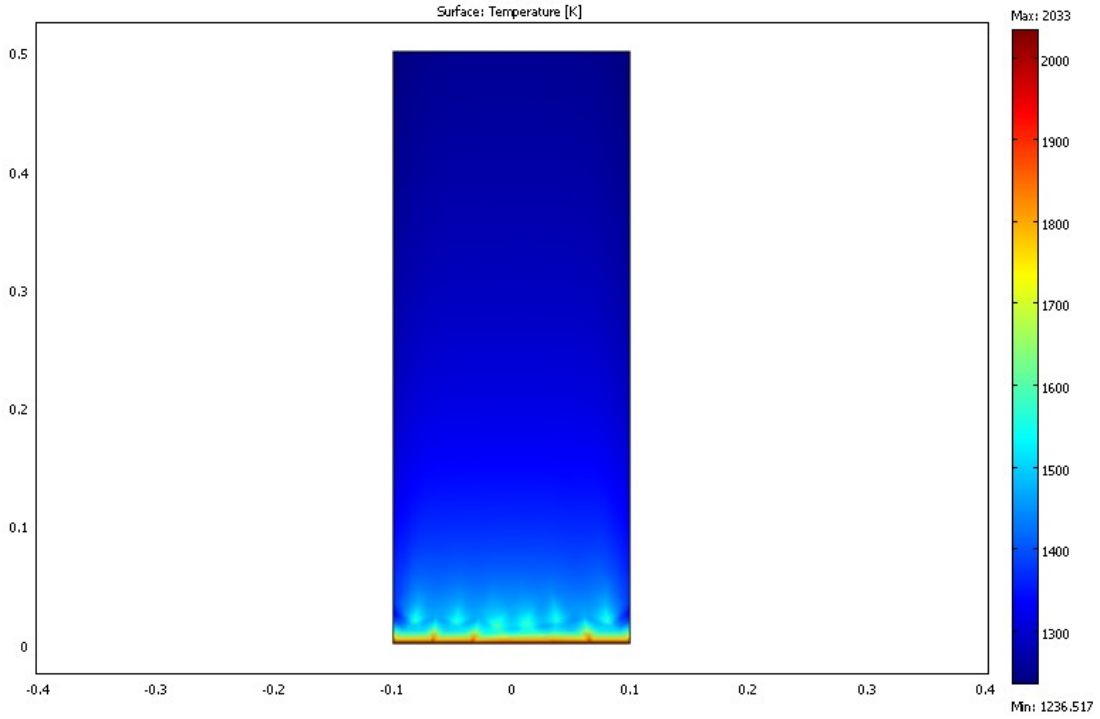

Figure M.5: Temperature profile in a fluidized bed with biogas as fuel

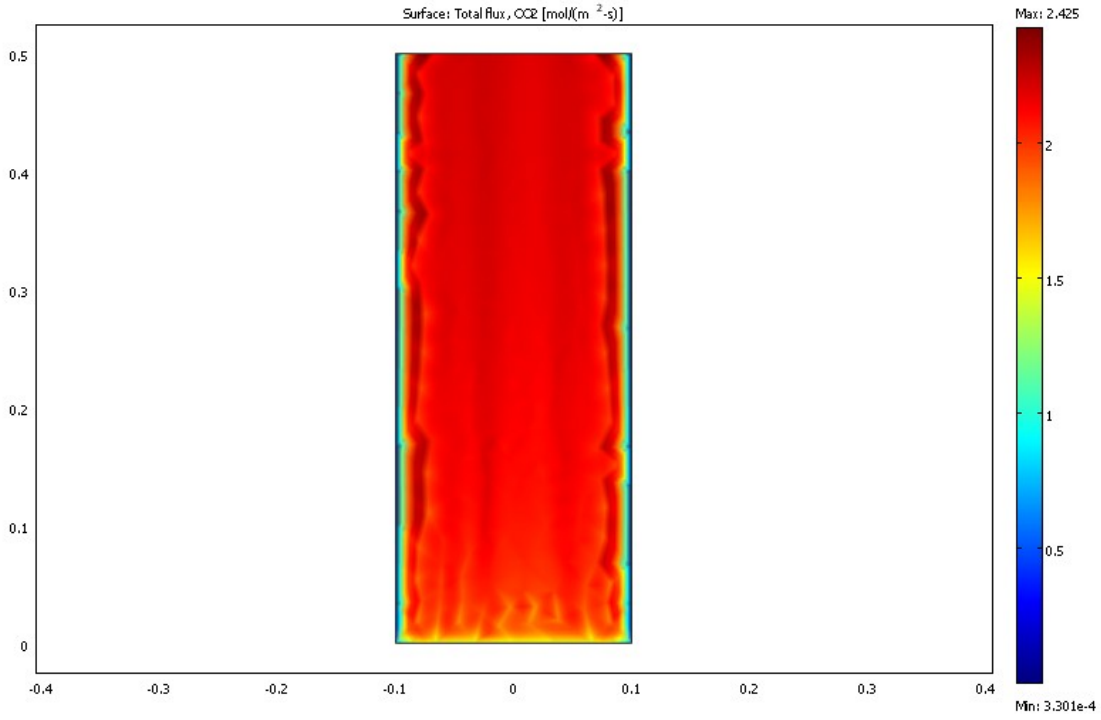

Figure M.6: CO_2 flux in a fluidized bed with SNG as fuel